Anisotropic Wrinkles of Graphene on Metal and Semiconductor Surfaces

by

Kam Sang Kwok

A thesis submitted to Johns Hopkins University in conformity with the requirements for the degree of Master of Science in Engineering

Baltimore, Maryland

Aug, 2017

Abstract

Graphene is a single layer of carbon with exceptional physical properties and chemical stability. The electronic band structure and chemical reactivity of graphene can be modified and enhanced by distorting the carbon-carbon bonds. Strained graphene exhibits different electrical, chemical and wetting properties from that flat graphene. However, controlling anisotropic wrinkles of graphene still remains challenging.

Here we propose new methods to create tensile strain in graphene on metal and semiconductor surfaces. Nanoscale and random graphene wrinkles were generated by the mismatch of thermal expansions of a bilayer. The bilayer comprised of aluminum (Al) or silicon (Si) and polymethyl methacrylate (PMMA) film, and graphene was then transferred on top of the bilayer. Random wrinkles were formed by heating the composite above the glass transition temperature of PMMA, due to the coefficient of thermal expansion of PMMA was greater than the Al and Si. In the end, strain in graphene was confirmed and quantified by the Raman spectra.

To control anisotropic wrinkles of graphene, two techniques were explored. The first technique applied polydimethylsiloxane (PDMS) molds on the surface of the composite during the heating process. The second patterned the Si (by photolithography and plasma etching prior transferring graphene. Both techniques generated few microns of wrinkles. We anticipated that both techniques would modify the chemical and electrical properties of graphene selectively.

Acknowledgments

I would like to thank Dr. Gracias for not only generously providing me with the opportunity and resources to work independently at Johns Hopkins University, but also guiding me in becoming a more creative and innovative researcher. I would like to thank Dr. Wang for agreeing to be the second reader for my thesis and the privilege of collaborating with his group. In addition, I would like to thank Dr. Pereira for my position as a teaching assistant.

I acknowledge support for my research from the National Science Foundation CMMI-1635443 and from the AFOSR.

I would like to thank Dr. Yang from the University of Illinois at Urbana-Champaign who provided the platform for me to explore and expand my knowledge in nanotechnology.

Last but not least, I would like to sincerely thank my parents and brother for supporting and encouraging me to pursue my dreams.

Figures

Tables

CHAPTER 1. Three-Dimensional Graphene

1.1. Fundamentals of Graphene

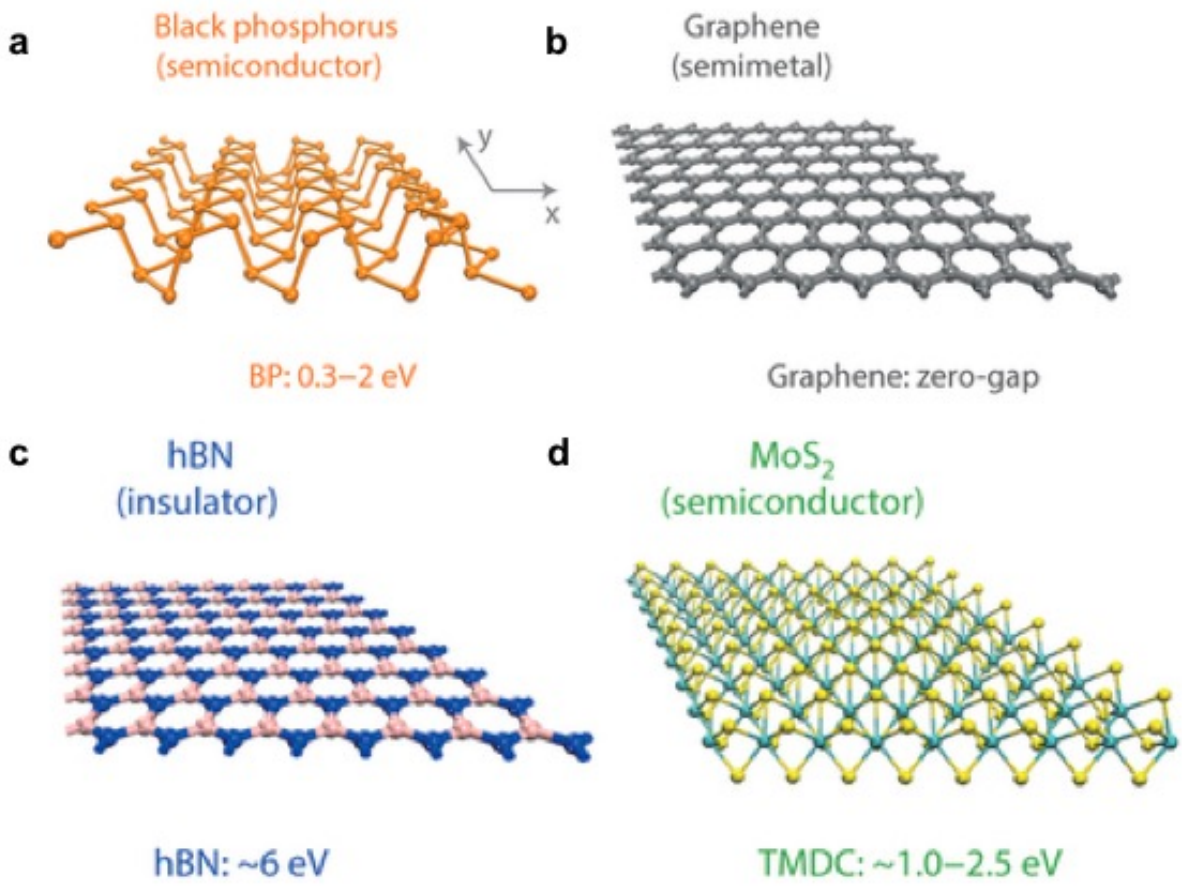

Figure 1. **Examples of Two Dimensional Materials. (a) Black phosphorus. (b) Graphene. (c) Hexagonal boron nitride. (d) Molybdenum disulfide. Reprinted by permission from Macmillan Publishers Ltd: Nature Photonic [1], copyright (2014)**

Graphene, a monolayer of sp^2 hybridized carbon atoms was first discovered in 2004 when Dr. Geim and Dr. Novoselov exfoliated graphite by Scotch tapes [19]. The discovery created numerous research opportunities globally, with more than 90,000 articles related to graphene related published, due to the remarkable properties and performance of graphene in various applications.

Table 1. **Physical Properties of Graphene [2].**

Hybridization	sp^2
Thickness (nm)	0.345
Young's Modulus (TPa)	1
Measured Surface Area ($m^2 g^{-1}$)	~1500
Optical Transmittance (%)	97.7
Thermal Conductivity ($W m^{-1} K^{-1}$)	4840-5300
Electrical Conductivity ($S cm^{-1}$)	2000

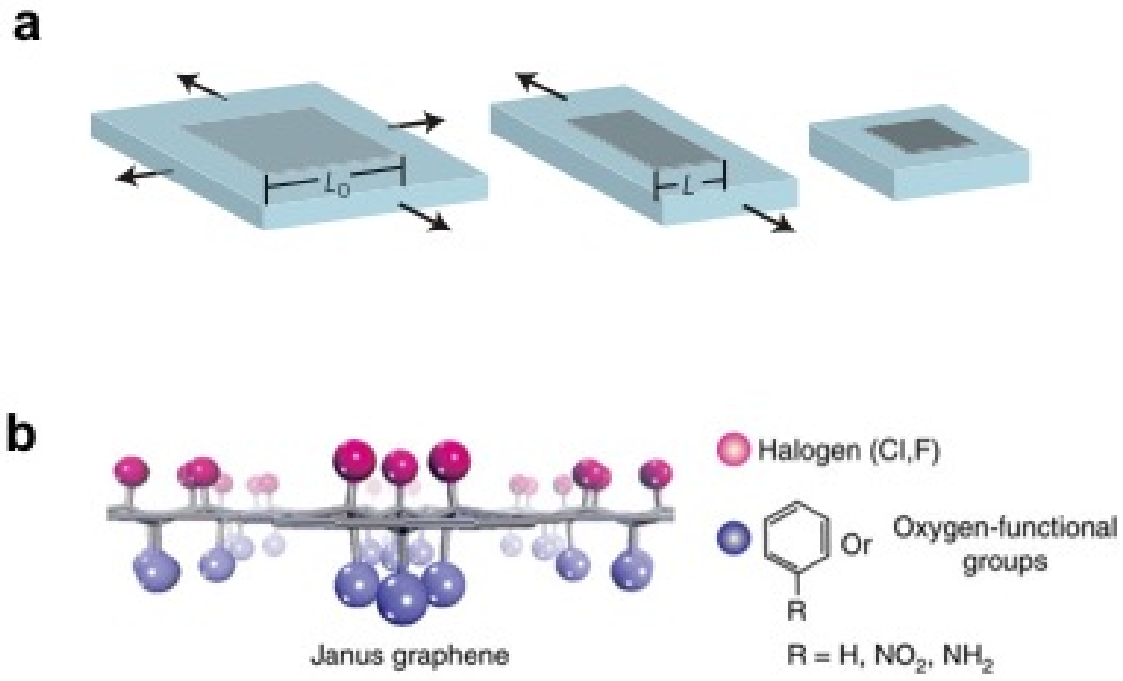

Figure 2. (a) Physical and (b) Chemical Approaches to Modify Properties of Graphene. Reprinted by permission from Macmillan Publishers Ltd: Nature Materials [3], copyright (2013) Reprinted by permission from Macmillan Publishers Ltd: Nature Communication [4], copyright (2013)

Graphene is a zero band gap material with high chemical resistance. The material is capable of sustaining extreme conditions, such as mechanical deformation and heat (Table 1) [2]. The intrinsic properties of graphene were ideal for operating in harsh environments, such as detecting

toxic chemicals and computer operations. To enhance the chemical reactivity and create band gap of graphene, strains can be introduced in graphene.

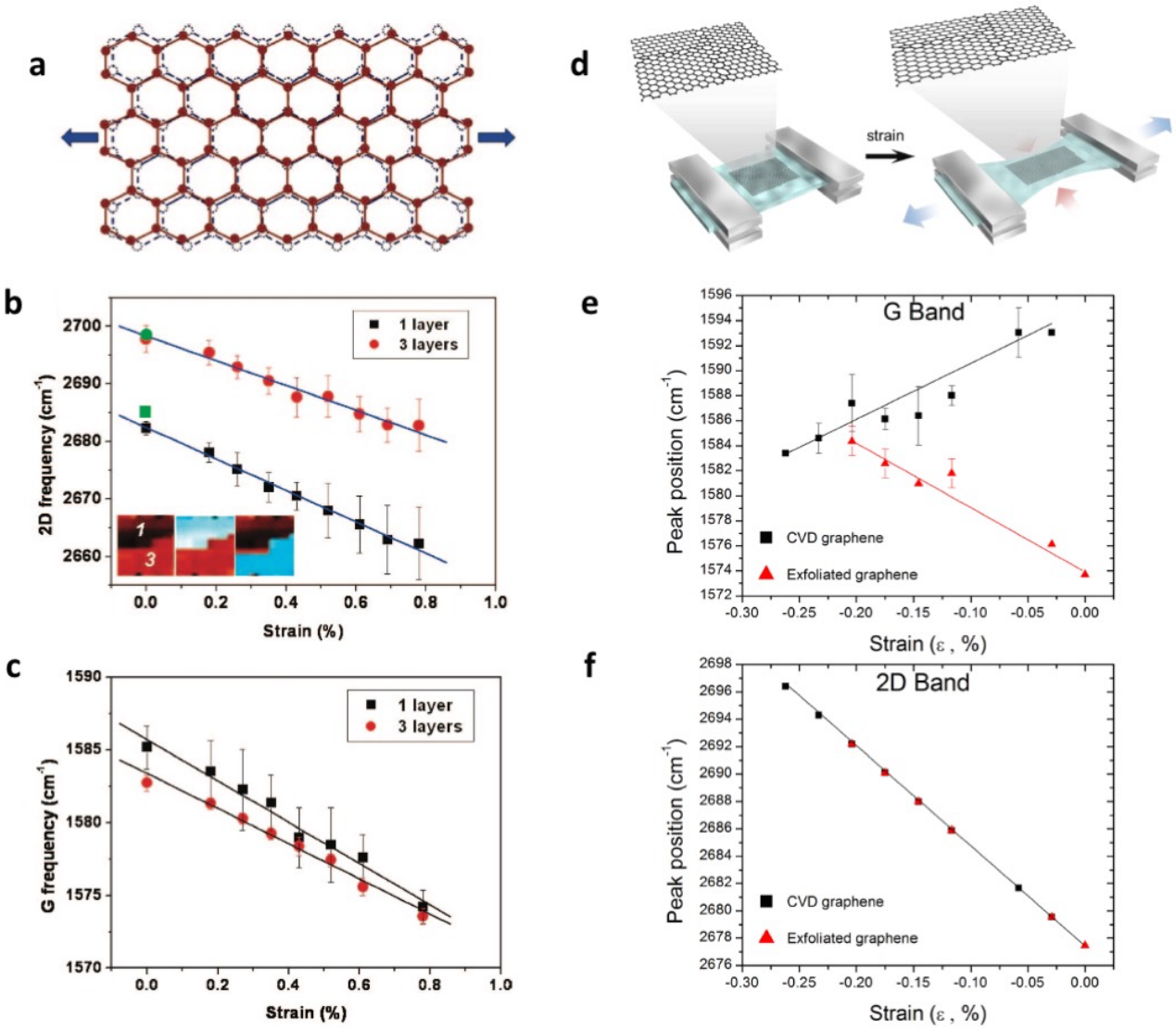

Figure 3. **Raman Spectra of Graphene under Tensile and Compressive Strains. (a) Scheme of graphene under tensile strain. (b-c) Raman spectra of graphene (1-3 layers) under tensile strain. (d) Graphene under tensile and compressive strain by stretching PDMS. (e-f) Raman spectra of graphene under tensile and compressive strain. Reprinted with permission from [5,6]. Copyright (2008,2012) American Chemical Society.**

Graphene is sensitive to external force, such as tensile and compressive forces [5,6]. Magnitude of tensile and compressive forces that act upon graphene can be characterized by Raman spectroscopy. Ni et al. analyzed how Raman spectra of graphene would be changed under uniaxial strain. (Figure 3. a-c). Graphene was first transferred on top of a polyethylene terephthalate (PET) film, and tensile strain (0-0.8%) was applied on the graphene by pulling PET in one direction. Red shifts of 2D and G bands were observed under tensile strain with slopes of the 2D and G bands found to be -27.8 cm^{-1} and –14.2 cm^{-1} per 1% strain respectively.

On the other hand, Bissett et al. demonstrated that graphene could be compressed by stretching polydimethylsiloxane (PDMS) (Figure 3. d-f) [5]. The 2D and G bands were shifted in an opposite direction when the PDMS was stretched, and the blue shift of the 2D band indicated that the graphene was under compressive strain (-0.30%). The compressive strain on the graphene was due to the high Poisson's ratio of PDMS, the compressive force was applied perpendicular to the direction of stretching the PDMS.

1.2. Applications of Strained Graphene

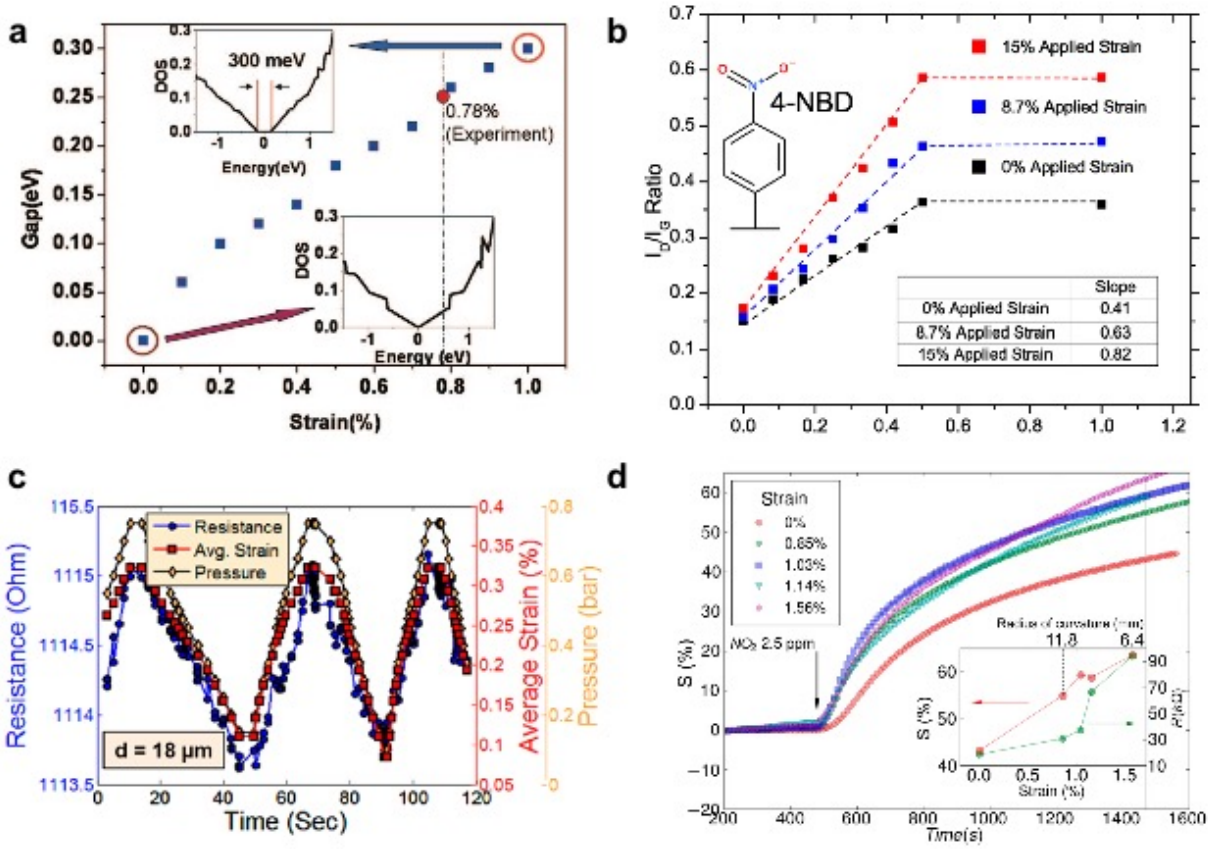

Figure 4. **Properties and Applications of Strained Graphene. (a) Calculated band gap of strained graphene. (b) Chemical reactivity of strained graphene. (c) Graphene pressure sensor. (d) Graphene gas sensor. Reprinted with permission from [5,7,8,9]. Copyright (2008, 2013, 2016, 2015) American Chemical Society**

Strained graphene has shown different physical and chemical properties than its relaxed state. For instance, Ni et al. calculated that band gap of graphene was directly proportional to tensile strain (Figure 4. a) [5], which suggested that strained graphene could served as a semiconductor. Although Ni et al. did not measure the electrical conductivity of the strained graphene, the work created a new research area to investigate the potential applications of strained graphene. Bissett et al altered the chemical reactivity of graphene by introducing compressive strain in graphene

(Figure 4. b) [7]. Three different aryl diazonuim salts were examined, and Bissett et al. observed a general trend that reactivity of graphene was enhanced significantly when compressive strain was applied. Bissett et al. believed that the compressive strain reduced the activation energy of the reaction.

Many applications have been developed by leveraging the properties of strained graphene, such as measuring gas pressure and sensing toxic gases. Smith et al studied how a suspended graphene on a cavity responded to gas pressure (Figure 4. c) [8]. Graphene was deformed when gas pressure was applied, which resulted tensile strain in graphene. The electrical resistance of graphene was found to be directly related to strain and pressure. The graphene sustained multiple cycles making it a good candidate as a gas sensor. In addition, Kumar et al. built a gas sensor sensitive to both mechanical strain and NO_2, a toxic gas (Figure 4. d) [9]. The gas senor was fabricated by simply transferring graphene on top of paper, and the sensitivity increased as the sensor was bent.

1.3. Methods to Fabricate Graphene Wrinkles

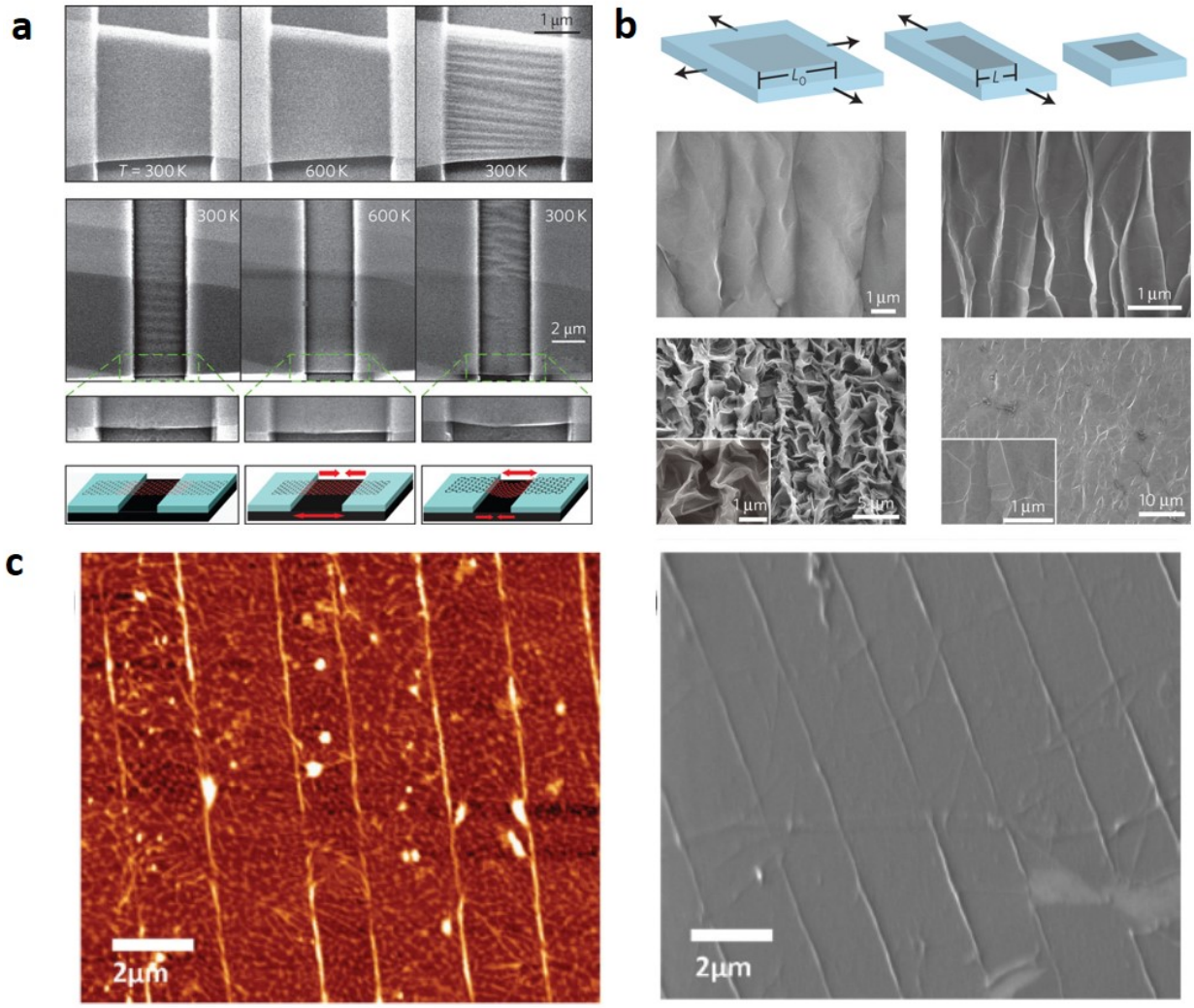

Figure 5. **Top-Down Techniques to Control Graphene Wrinkles. (a) Thermal expansion. (b) Pre-stretched elastomer. copyright (2013) Reprinted by permission from Macmillan Publishers Ltd: Nature Nanotechnology [10], copyright (2009) Reprinted by permission from Macmillan Publishers Ltd: Nature Material [3], copyright (2013), Copyright © (2013) by John Wiley & Sons, Inc. Reprinted by permission of John Wiley & Sons, Inc [11].**

Strained graphene has excellent prospects in different applications, however deploying strained graphene in practical applications remains challenging. To maintain uniform strain in graphene, nano and micro fabrications play an important role. This section covers versatile top-down techniques to reserve strain in graphene by creating graphene wrinkles with precision.

Periodic wrinkles of graphene were first demonstrated by Bao et al [10], and graphene wrinkles were formed due to a mismatch of thermal expansion between graphene and Si/SiO_2. Graphene was suspended on Si/SiO_2 trenches, and graphene wrinkles were observed after thermal annealing. The wrinkles were produced in the direction that was perpendicular to the silicon trenches (Figure 5. a). To study the reversibility of wrinkled and crumpled graphene, Zang et al. transferred graphene on pre-stretched elastomers (Figure 5. b) [3]. Wrinkles and Crumples of graphene were made by releasing the elastomers uniaxially and biaxially respectively.

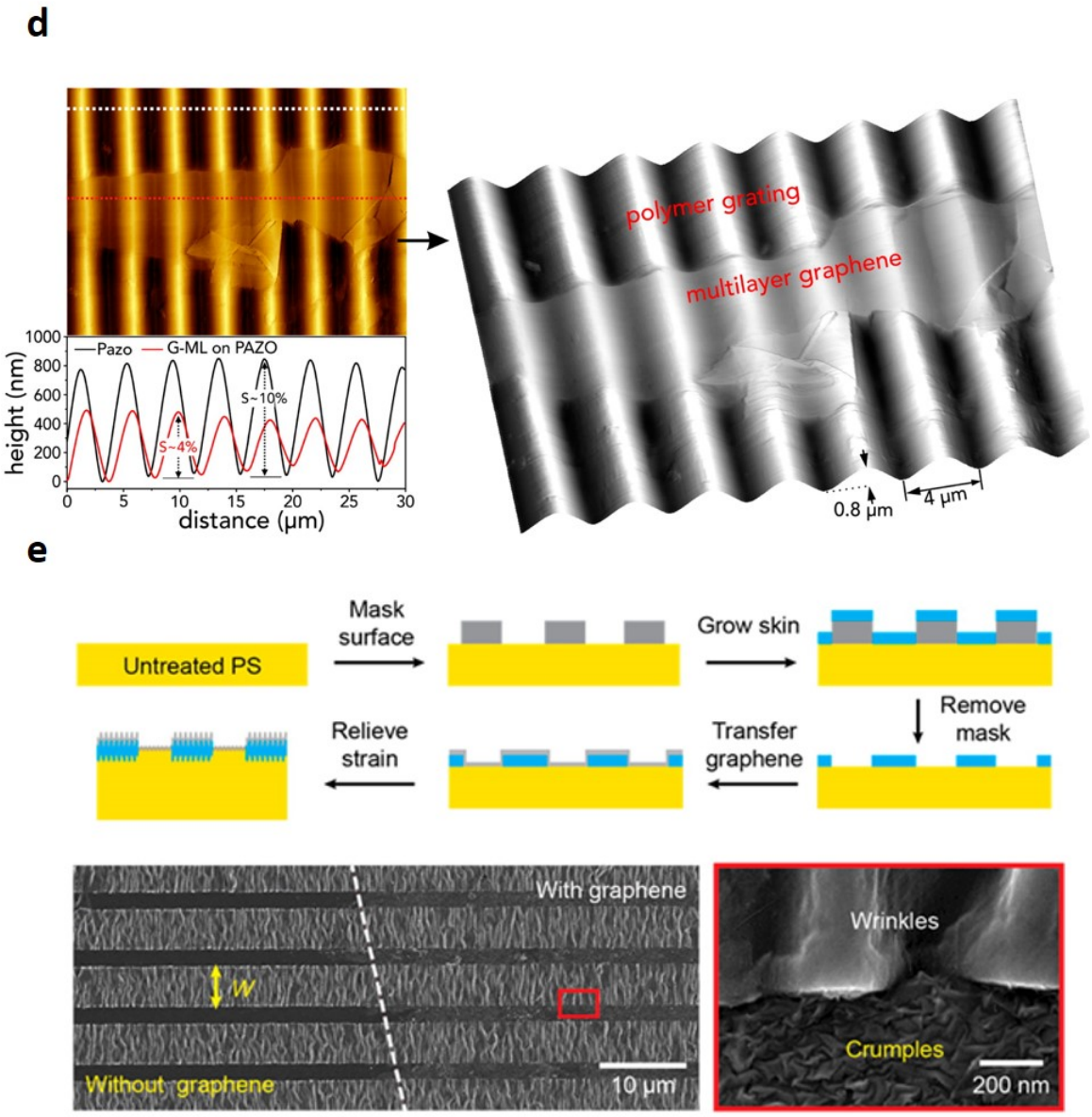

Figure 5. **Top-Down Techniques to Control Graphene Wrinkles. (d) Photopolymer. (e) Heat-shrink polymer. Reprinted with permission from [12,13]. Copyright (2014, 2016) American Chemical Society.**

Further research exploring the manipulation of anisotropic graphene wrinkles have been conducted by different groups. Hallam et al. showed that folded graphene were printed on wafers by patterned elastomeric stamps (Figure 5. c) [11]. The width of the wrinkles was less than 25 nm and the length was between 30 and 120 nm. To achieve continuous and uniform wrinkles of graphene, shape

memory polymers were utilized. Florio et al. deposited graphene on a photosensitive polymer film, and the graphene partly adapted the shape of the photosensitive polymer after the film exposure to the laser (Figure 5. d). Recently, Lee et al. wrinkled graphene on commercially available heat-shrink polymer substrates. Homogeneous graphene wrinkles were tuned from nano to micro scales, and different wavelengths of graphene wrinkles were achieved selectively on the same substrate.

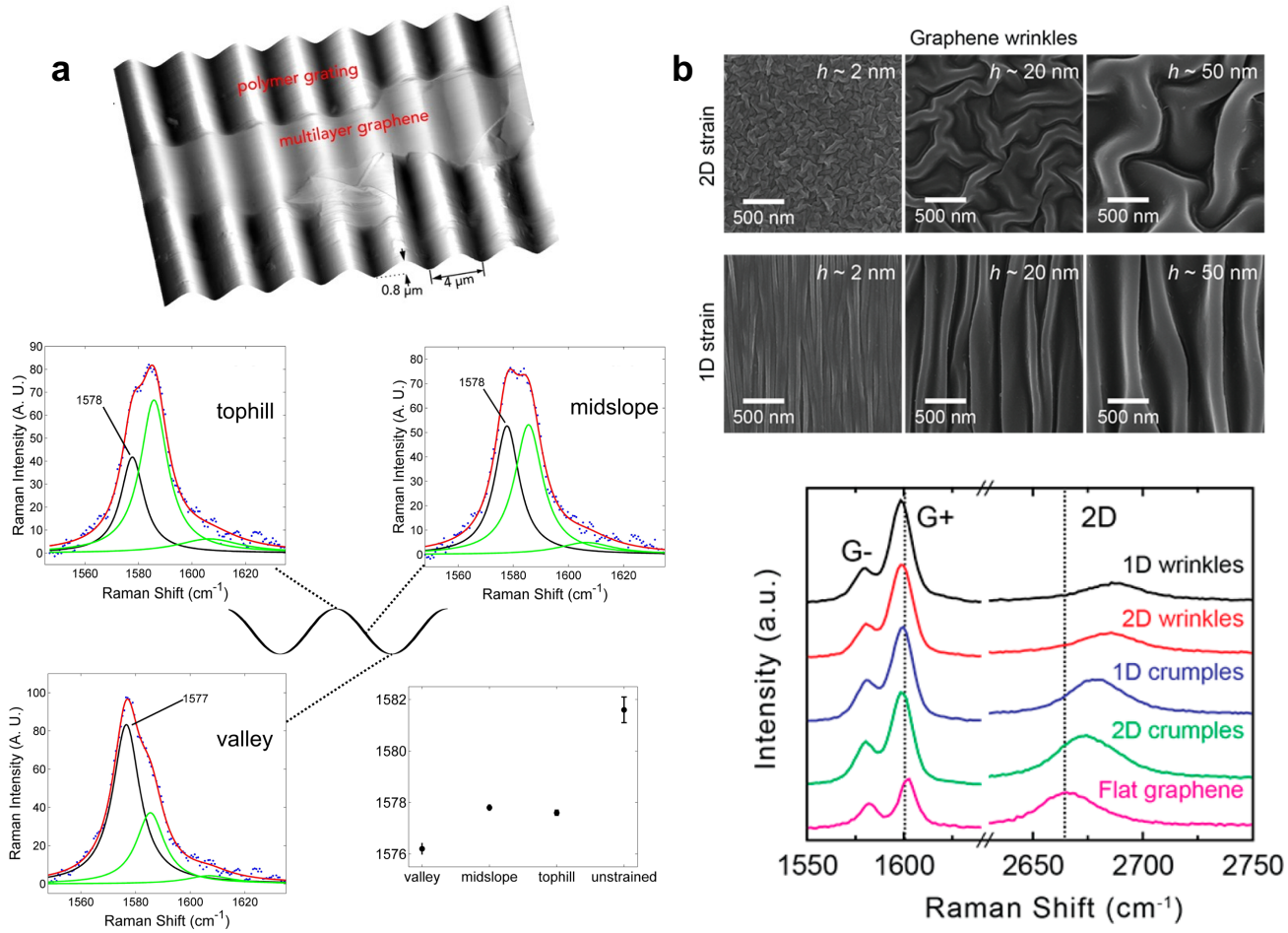

Figure 6. **Raman Spectra of Graphene Wrinkles. (a) Tensile strain on graphene by photopolymer and (b) Compressive strain on graphene by heat-shrink polymer. Reprinted with permission from [12,13]. Copyright (2014, 2016) American Chemical Society.**

Tensile or compressive strain was found in graphene wrinkles. For example, Florio et al. observed that different degrees of tensile strain were found in the graphene wrinkles (Figure 6. a) [12], and the G band of the graphene wrinkles was red shifted. In addition, graphene wrinkles experienced more tensile strain at the valley of the polymer grating than in comparison with different locations agreement with the previous result. Compressive strain in graphene wrinkles was detected on top of heat-shrink polymer substrates, and the 2D band of the graphene wrinkles was blue shifted significantly [13].

In conclusion, tensile or compressive strain in graphene can be generated by different approaches according to the Raman spectra. Top-down techniques that utilized polymer substrates produced good quality and high yield of graphene wrinkles (Figure 6. b, d-e). The Raman spectra suggests that increasing the surface area of a substrate can create tensile strain in graphene, and reducing the overall volume of a substrate can yield compressive strain in graphene.

CHAPTER 2. Strategies to Wrinkle Graphene on Metal and Semiconductor Surfaces

2.1. Introduction

Graphene wrinkles have received much attention and opened up numerous research opportunities as discussed in the previous chapter. However, only suspended graphene wrinkles and graphene wrinkles on polymer substrates were explored. Many studies revealed that graphene can be influenced chemically by metal and semiconductor. For instance, Wang et al showed that chemical reactivity of graphene can manipulated by the underlying substrate [28]. In comparison with semiconductor and insulator substrates, the chemical kinetic of graphene supported on Al_2O_3 and SiO_2 had enhanced. In this chapter, a process that generated isotropic and anisotropic metal and semiconductor wrinkles was demonstrated, including experiments and simulations. The technique to wrinkle metal and semiconductor surfaces was utilized to produce graphene wrinkles in the next chapter.

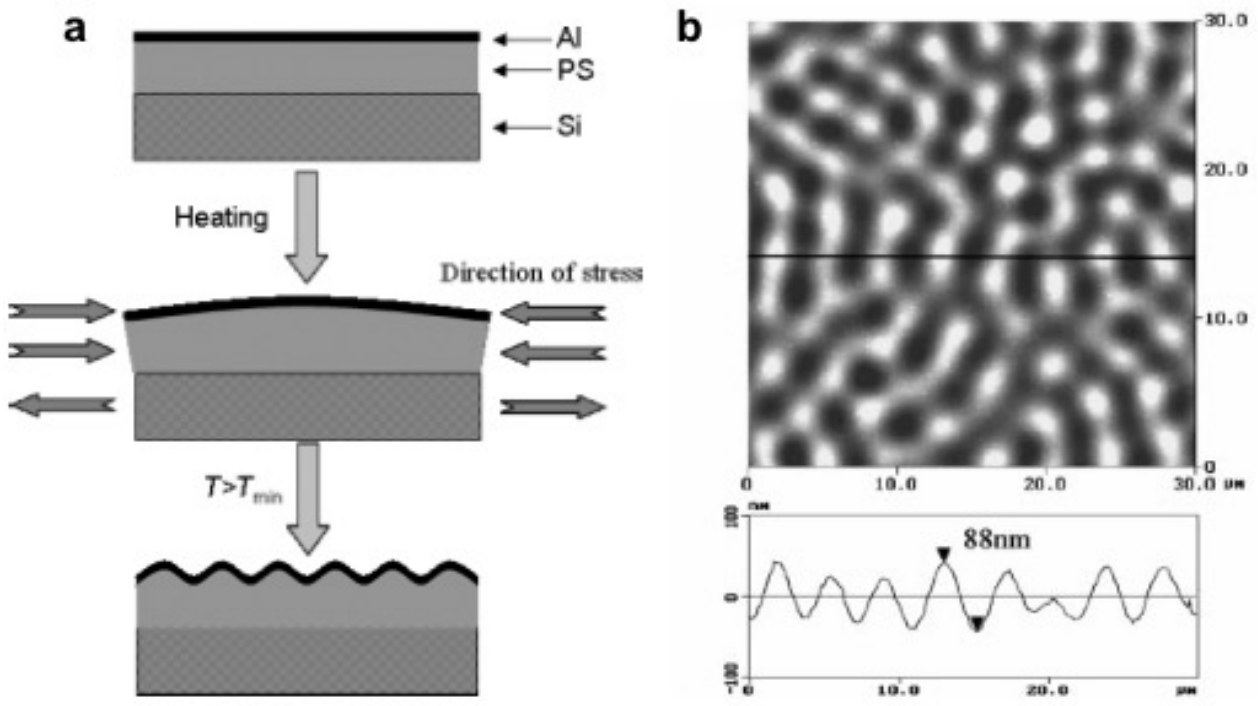

***Figure 7*. Formation of Al Wrinkles due to mismatch of thermal expansion between the top and bottom materials. (a) Scheme of produce Al wrinkles due to mismatch of thermal expansions. (b) AFM images of Al wrinkles. Copyright © (2004, 2002) by John Wiley & Sons, Inc. Reprinted by permission of John Wiley & Sons, Inc [14, 15].**

Ordered wrinkles of metal surfaces was first discovered by Bowden et al. in 1998, and the wrinkles were driven by the mismatch of thermal expansion and Young's module between gold and elastomeric substrate (PDMS) [16]. The Au layer avoided the expanded PDMS to return its original size, because the coefficient of thermal expansion of PDMS is greater than gold (Au), and and the Young's modulus of Au is larger than PDMS. A thin layer of Au was deposited on top on a PDMS via thermal evaporation, and sufficient heat caused the PDMS to expand during the deposition. Au wrinkles were generated when the gold and PDMS layers reached room temperature.

A similar approach to generate wrinkles was shown by Yoo et al (Figure 7. b), and anisotropic wrinkles were aligned by soft lithography [15]. A thin polystyrene (PS) film was first deposited on a silicon wafer by spin-coating. A 50 nm of aluminum (Al) was evaporated on top of the PS film. PS has higher glass transition temperature (>100 ^{o}C) than PDMS, so PS did not expand during the evaporation. The Al wrinkles were generated by heating the substrate above the glass transition temperature of the PS film (Figure 7. a). To align the wrinkles, patterned PDMS stamps (e.g. lines and squares) were placed on top of the substrate during the annealing process (Figure 8.).

Recent studies show that nanoscale metal wrinkles can be achieved by reducing the thickness of metal and polymer layers. Zhang et al produced wrinkles with wavelengths of about 500 nm. Instead of depositing 50 nm of Al, 5 nm of Au were evaporated on top of an ultrathin PS film [17]. Also, the experimental results had a good agreement with the theoretical calculation. From the same group, Guo et al developed an innovative technique to direct the Au wrinkles [18]. The bilayer was patterned by laser direct writing, and anisotropic wrinkles were created by heating above the glass transition temperature of PS. The Young's modulus in the laser- exposed area was reduced, and the wrinkles were found in the unexposed area.

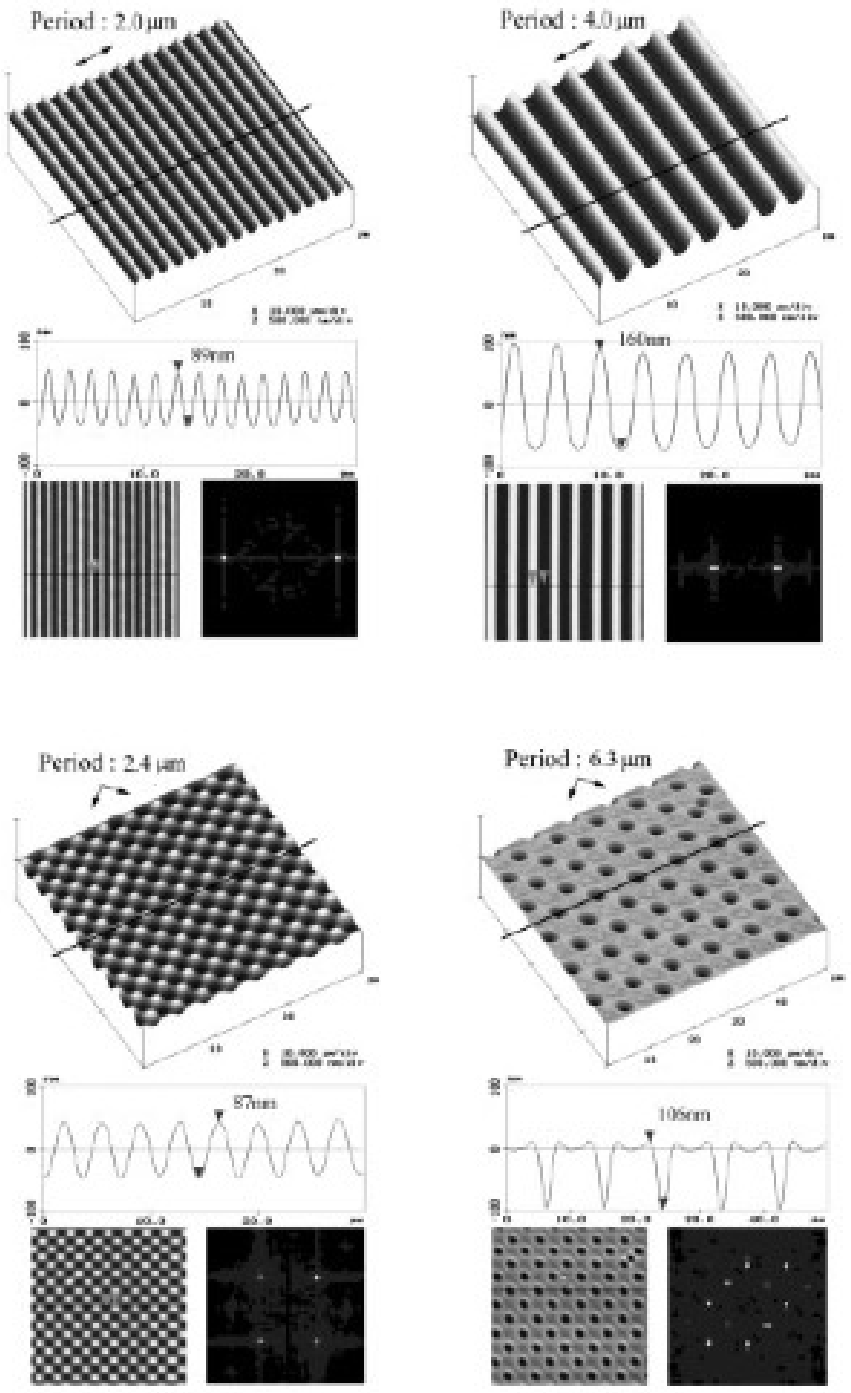

***Figure 8*. Aligning Al Wrinkles by Soft-lithography. Copyright © (2002) by John Wiley & Sons, Inc. Reprinted by permission of John Wiley & Sons, Inc [15].**

Here we demonstrated a new method to create and manipulate wrinkles of silicon (Si) and polymethy-methacrylate (PMMA). PS was substituted with PMMA, because uniform PMMA can be easily prepared by spin-coating. In addition, PMMA has similar thermal properties as PS, such as thermal expansion and glass transition temperature. In previous studies, only metals were examined as the top layer. However, measuring electrical conductivity of graphene wrinkles on metal surfaces would be challenging. Instead of evaporating metals on PMMA, Si was deposited. In the end, aligning and controlling Al and Si wrinkles were explored. Si wrinkles were guided by combing photolithography and plasma etching.

2.2. Experimental Section

Fabrication of Metal/ Semiconductor and Polymer Bilayer

The bilayer was prepared in two steps. Initially, different thickness (100 – 800 nm) of Polymethyl-methacrylate (PMMA, 950K A Resist) on top of silicon wafers were prepared by spin-coating. The thickness of the PMMA film was controlled by the concentration of PMMA (2 -7%) and the spinning speeds (500 – 6000 rpm). PMMA on the wafer was baked at 125 ℃ for 1 minute to remove excess solvent.

Aluminum (Al) or silicon (Si) with a thickness of 50 nm was deposited on top of the PMMA by thermal evaporation. Silicon wafers were used as the silicon source. Briefly, materials were deposited when the vacuum chamber reached 1×10^{-5} psi, and the deposition rate was maintained at 0.5 Å per second.

Formation of Al and Si Micro-Wrinkles

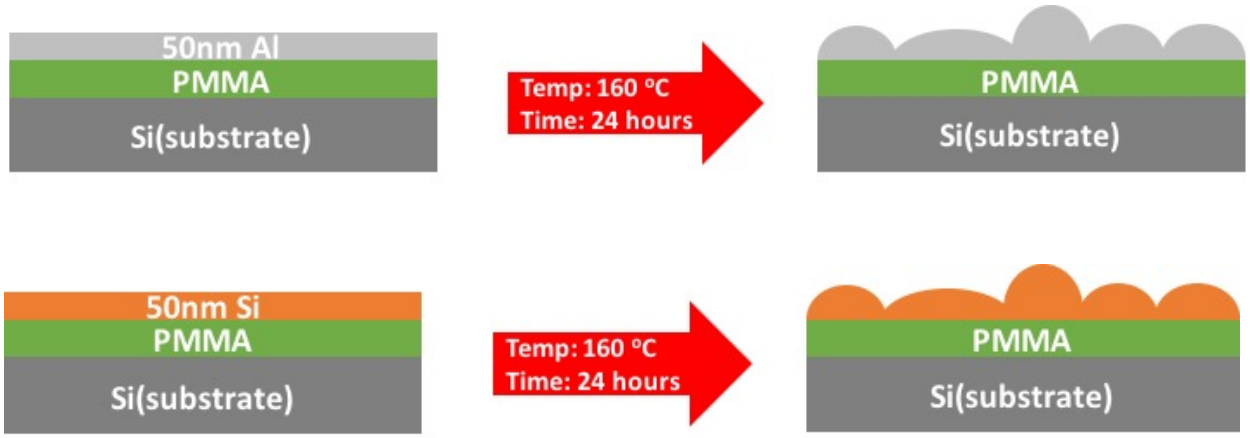

***Figure 9*. Formation of Al or Si Wrinkles in This Work.**

The bilayer was heated on top of a hot plate in an ambient environment for 24 hours, and the annealing temperature ranged from $120 - 190$ ℃ (Figure. 9). The wrinkles were examined by optical microscopy and atomic force microscopy (AFM).

Aligning Wrinkles by Soft-lithography

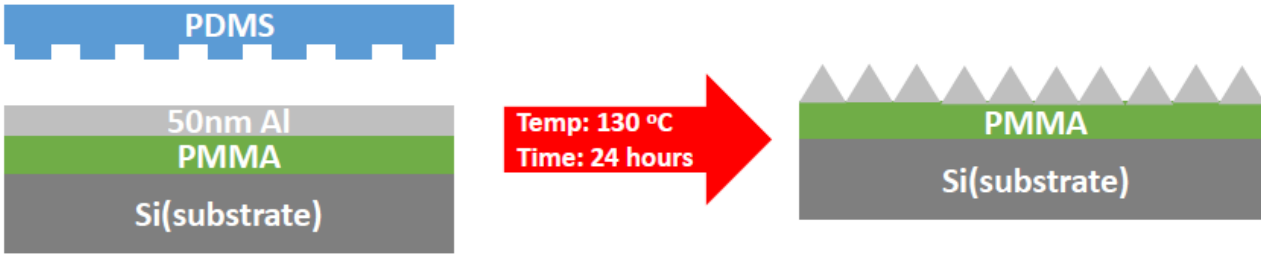

***Figure 10.* Schematic of Aligning Al Wrinkles by Soft-lithography**

Photolithography was utilized to fabricate the molds of the PDMS stamps. First, positive photoresist (MicroChem1805) was spun on top of a silicon wafer at 3000 rpm. After spin coating, the wafer was soft baked on a hotplate at 125 ℃ for one minute. Features were created via exposure of the wafer to UV light within the mask aligner at an intensity of 50 mJ/cm^2. Finally, the wafer was immersed in the developer (MC-351) for one minute, and rinsed and dried with water and nitrogen.

The stamps to align wrinkles were constructed using PDMS and the photoresist masters. A premixed PDMS solution (10:1) was poured into a petri dish with the masters at 90 ℃ for two hours. The patterned stamps were peeled off from the photoresist masters and placed directly on top on the bilayer. Aligned wrinkles were formed by annealing the bilayer at $120 - 190$ ℃ for 24 hours.

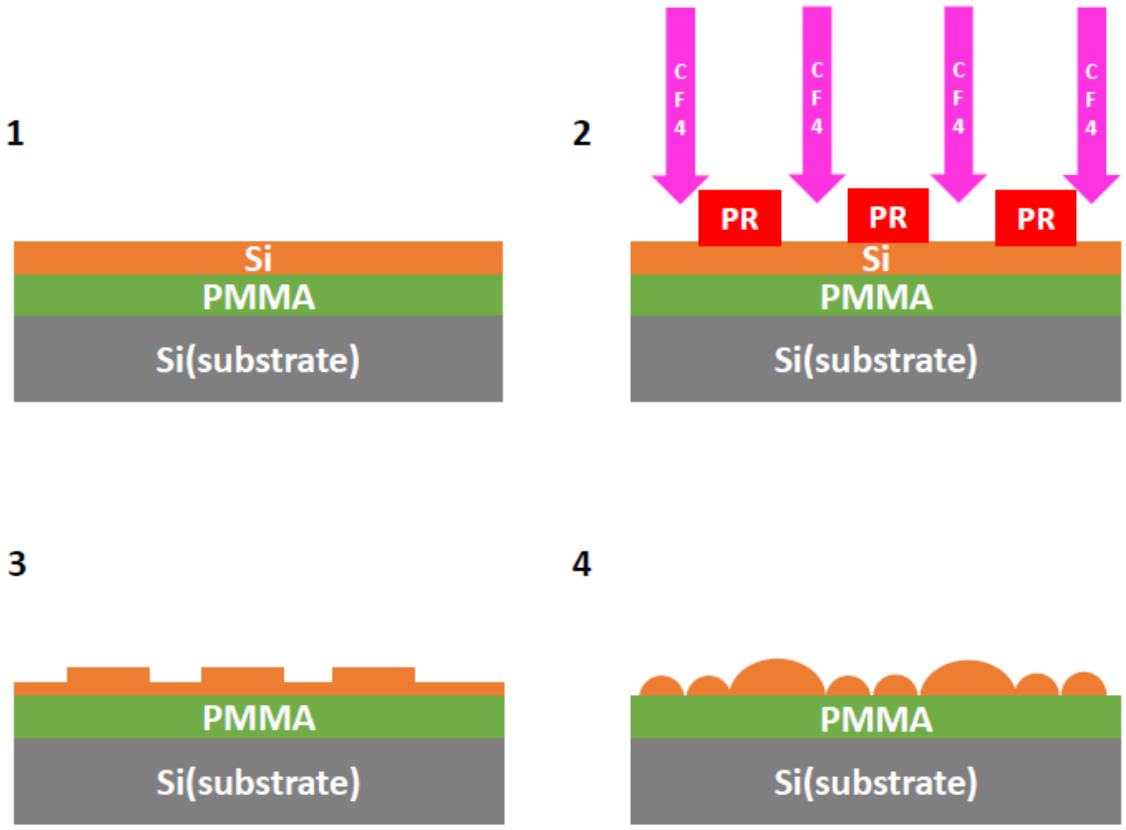

Figure 11. **Schematic of Plasma Assisted Wrinkles**

Patterns of positive photoresist (MicroChem 1805) were fabricated on top of the Si and PMMA bilayer. The bilayer was inserted into the plasma etcher (60 watts, O_2: 2 sccm, CF_4: 20 sccm) for 1 – 10 minutes. The photoresist was then removed by rinsing isopropanol. Patterns of wrinkles were formed by annealing the bilayer at 120 ℃ for 24 hours.

2.3. Results and Discussion

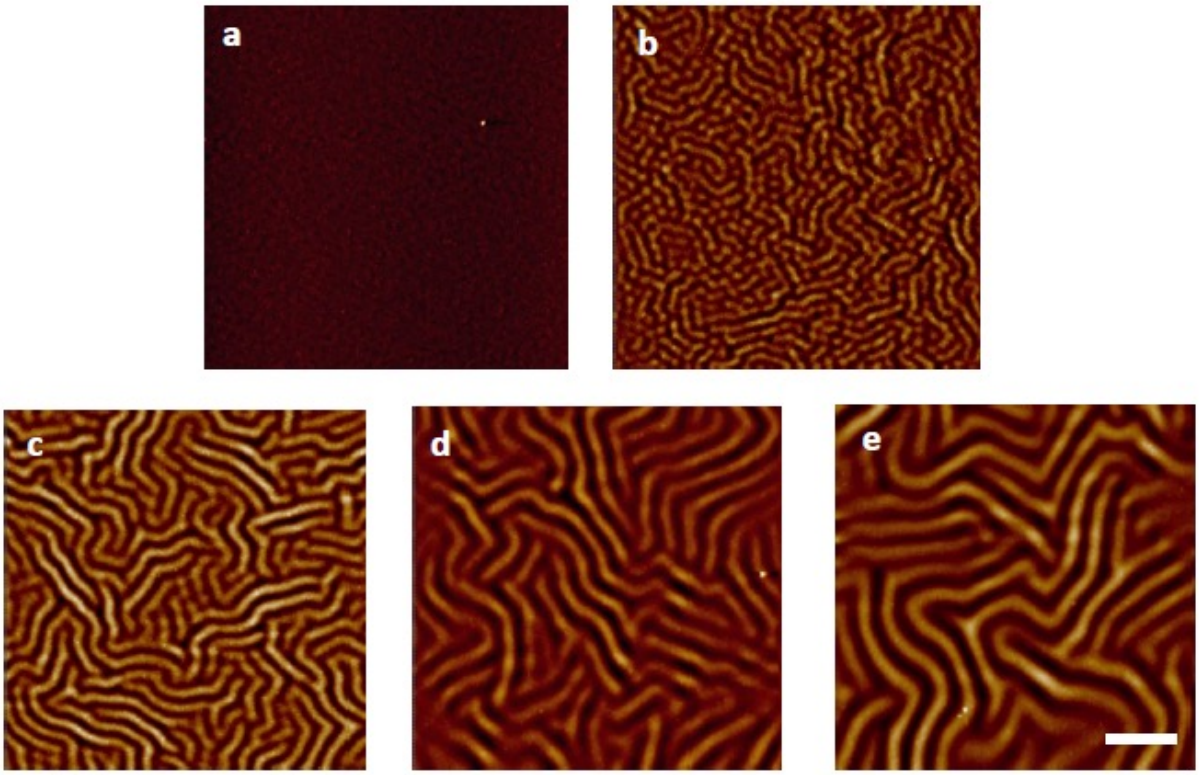

***Figure 12*. AFM images of Controlling the Morphologies of Al Wrinkles by Varying the Thickness of PMMA. (a) 100 nm. (b) 200 nm. (c) 400 nm. (d) 600 nm. (e) 800 nm. The scale bar is 10 um.**

PMMA as the polymer layer can be used to create Al wrinkles (Figure 12), and the results were in accordance with the observation of Yoo et al. The wavelengths and heights of the Al wrinkles were directly proportional to the thickness of PMMA. Initially, no Al wrinkles were found at the sample with 100 nm of PMMA (Figure 12. a), discontinuous Al wrinkles and dots appeared on 200 nm of PMMA. Continuous Al wrinkles were observed at 400 nm of PMMA, and Al wrinkles were enlarged as increasing the thickness of PMMA. Figure 13 presented the summary of the

relationship between the thickness of PMMA (200 – 800 nm), wavelength or height of the Al wrinkles.

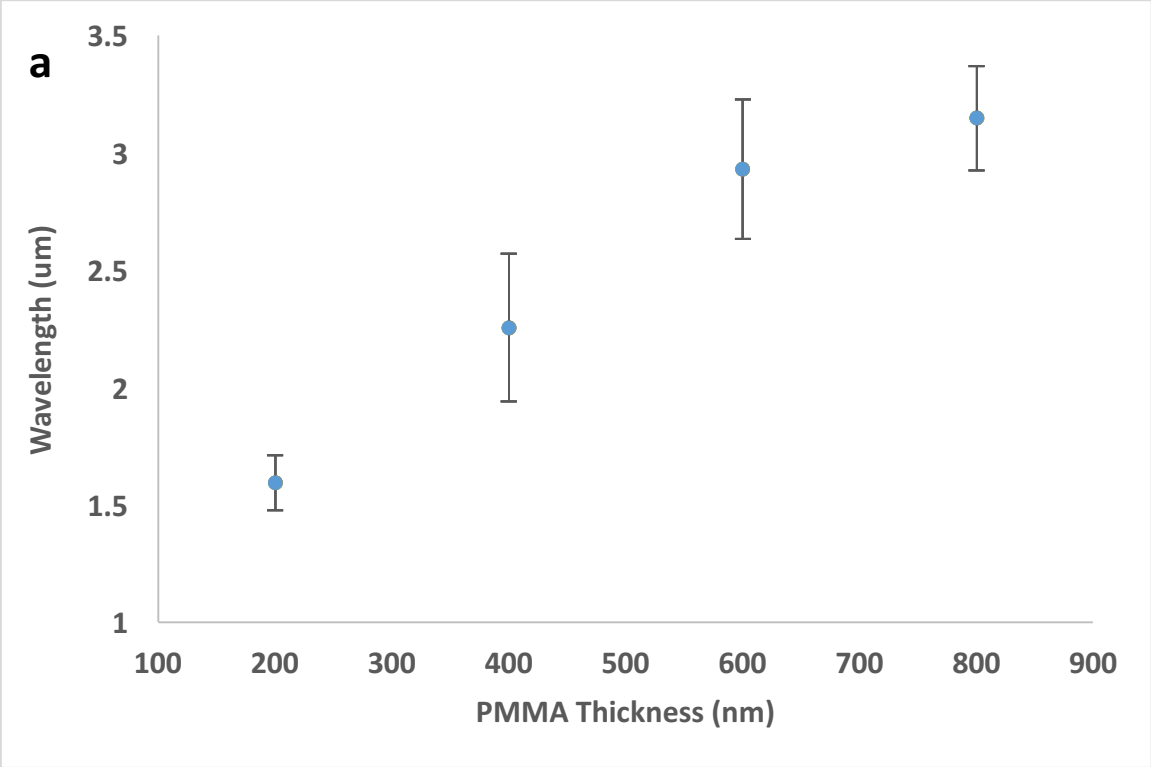

***Figure 13*. Measurement of Al Wrinkles with Different Thickness of PMMA. (a) Wavelengths of the Al wrinkles**

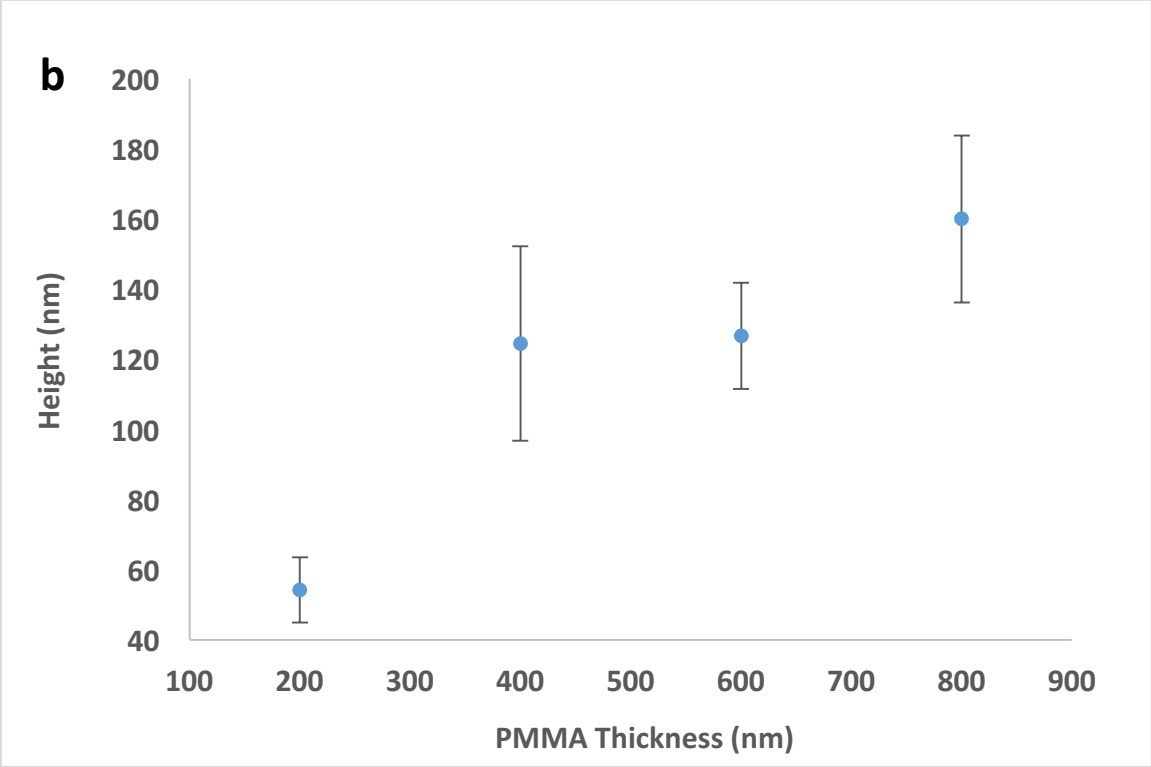

***Figure 13*. Measurement of Al Wrinkles with Different Thickness of PMMA. (b) Heights of the Al wrinkles.**

Wavelengths of the Al wrinkles were computed. Yoo et al derived the equation (1) to predict wavelengths of Al wrinkles by correlating the physical properties of metal and polymer, and the equations were expressed as follows [15]:

$$\lambda = 2\pi t_m \left(\frac{Y}{1+\sqrt{1+12YH^3}}\right)^{\frac{1}{3}} \quad \ldots\ldots (1)$$

$$Y = \left(\frac{1}{2(1-v_m^2)}\right)\left(\frac{E_m}{E_p}\right) \quad \ldots\ldots (2)$$

$$\log\frac{E_p}{E_{p0}} = \frac{-C_1(T-T_0)}{C_2 + ((T-T_0)} \quad \ldots\ldots(3)$$

$$H = \frac{t_m}{t_p} \ldots\ldots(4)$$

By assuming PMMA had similar characteristics as PS, Young's modulus and Williams- Landel-Ferry constants of PS were applied in the calculations. All the values are listed in Table 2, and the theoretical model and experiential measurements are shown in Figure 14.

***Table 2*. Summary of Al and PMMA Properties [15].**

Wavelength	λ	
Thickness of Metal	t_m	50 nm
Thickness of Polymer	t_p	200 – 800 nm
Young's modulus of metal	E_m	70 GPa
Young's modulus of polymer at the glass transition temperature	E_{p0}	3.2 GPa
Young's modulus of polymer at given temperature	E_p	
Poisson ratio of Metal	v_m	0.33
Williams-Landel-Ferry constant	C	$C_1 = 12.7, C_2 = 49.8\ K$
Annealing temperature	T	1
Glass transition temperature	T_0	378 K

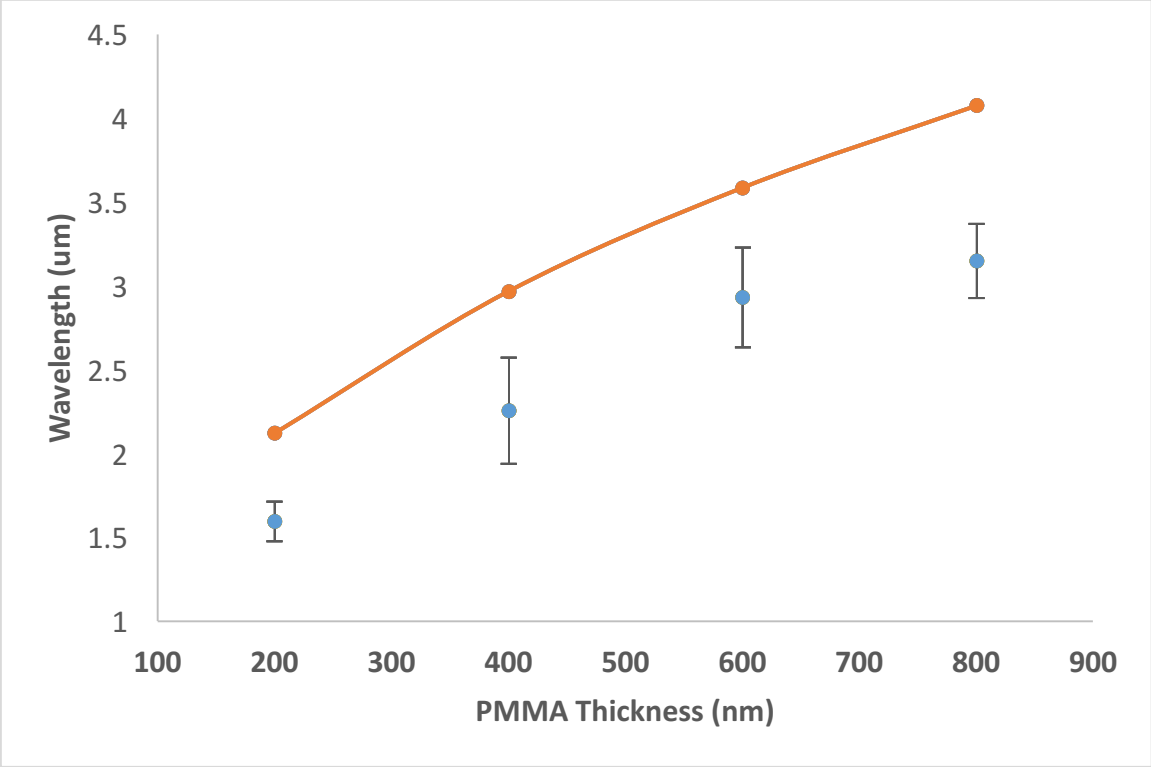

***Figure 14*. Comparison of Predicted and Measured Al Wrinkles. Predicted Al Wrinkles (Orange line) and Measured Al Wrinkles (Blue dots).**

The trend of the Al wrinkles was predicted (Figure 14), and the simulation contained about 25% error. The theoretical model was sensitive to the thickness of Al, PMMA and the Young's modulus of PMMA. The thickness of Al and Young's modulus of PMMA caused the major error in the simulation. Evaporating a uniform Al film was extremely difficult due to the limitation of the deposition. Accuracy of the model would be greatly improved by obtaining a measured Young's modulus of PMMA at the annealing temperature, however complex system would be required.

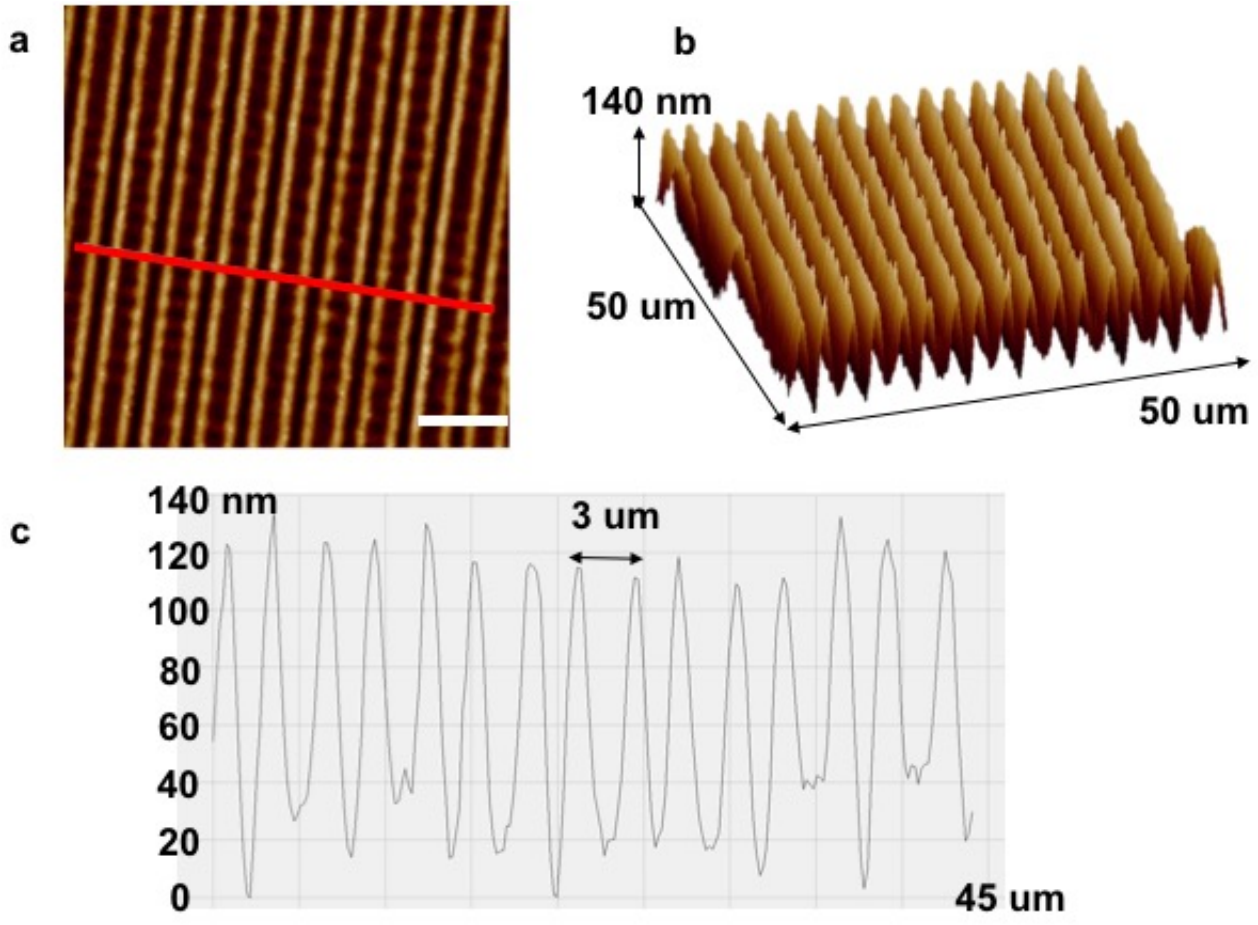

Figure 15. **Aligning Al Wrinkles (50 nm Al and 600 nm PMMA) by Soft-lithography. The scale bar is 10 um.**

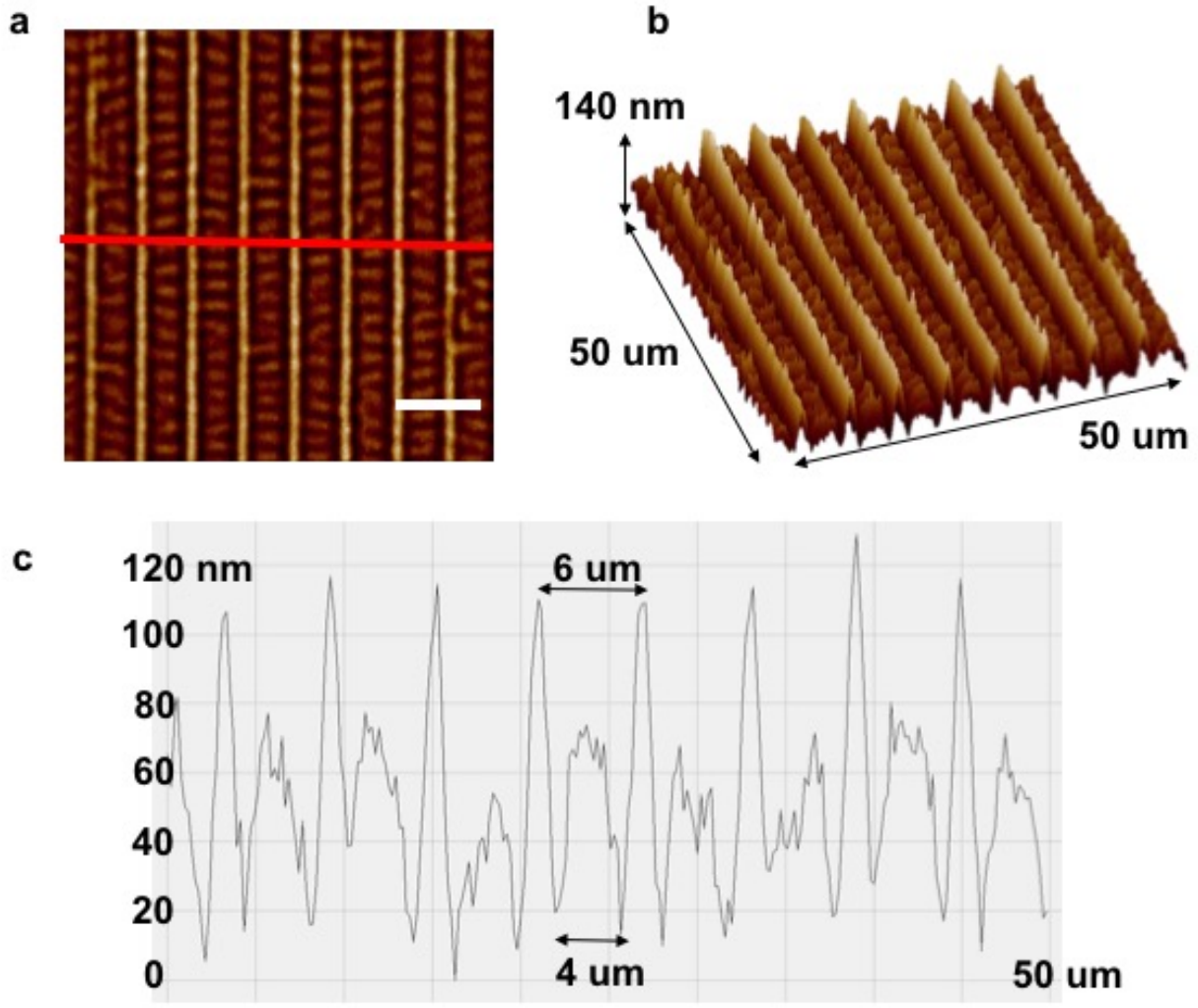

Figure 16. **Aligning Al Wrinkles (50 nm Al and 800 nm PMMA) by Soft-lithography. The scale bar is 10 um.**

Aligning Al wrinkles by soft lithography was first demonstrated by Yoo et al [15], and aligned Al wrinkles can be reproduced using PMMA. Morphologies of aligned Al wrinkles were controlled by varying the thickness of PMMA, and the results were matched with the findings of Yoo et al. Periodic Al wrinkles with 3 um spacing were created by using 3 um lines PDMS mold on the bilayer (Figure 15). The spacing between the Al wrinkles became wider when 800 nm of PMMA was used.

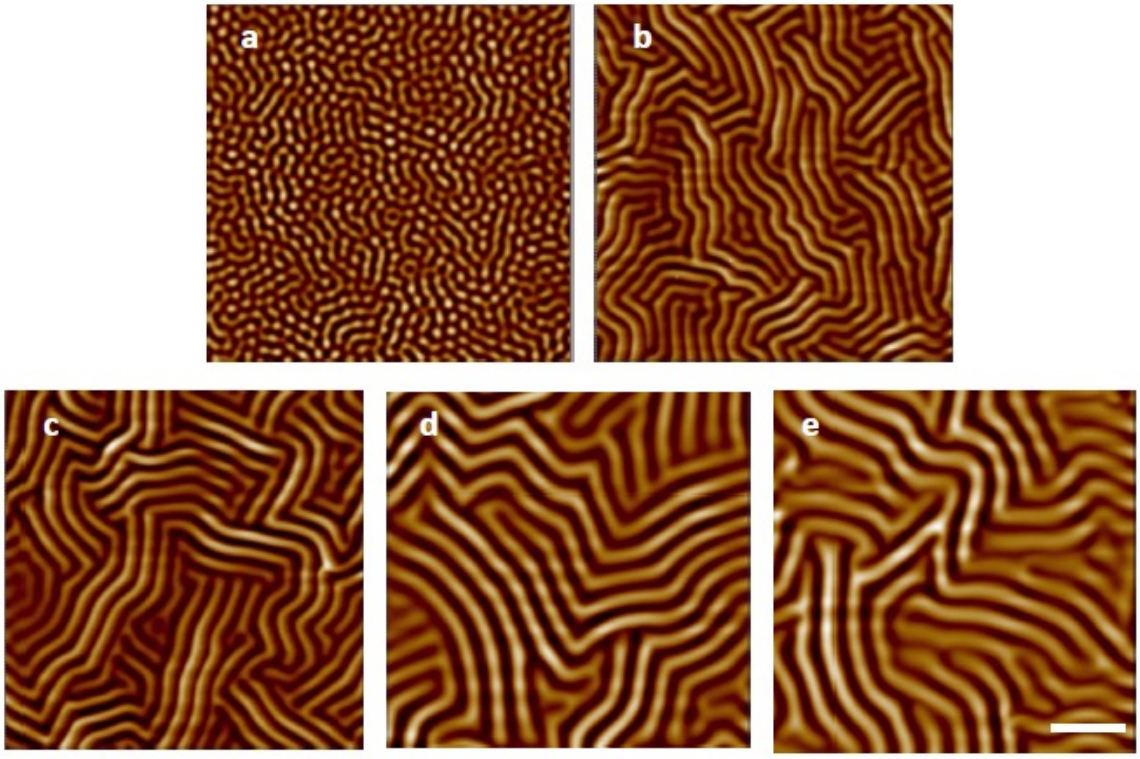

Figure 17. **AFM images of Controlling the Morphologies of Si Wrinkles by Varying the Thickness of PMMA. (a) 100 nm. (b) 200 nm. (c) 400 nm. (d) 600 nm. (e) 800 nm. The scale bar is 10 um.**

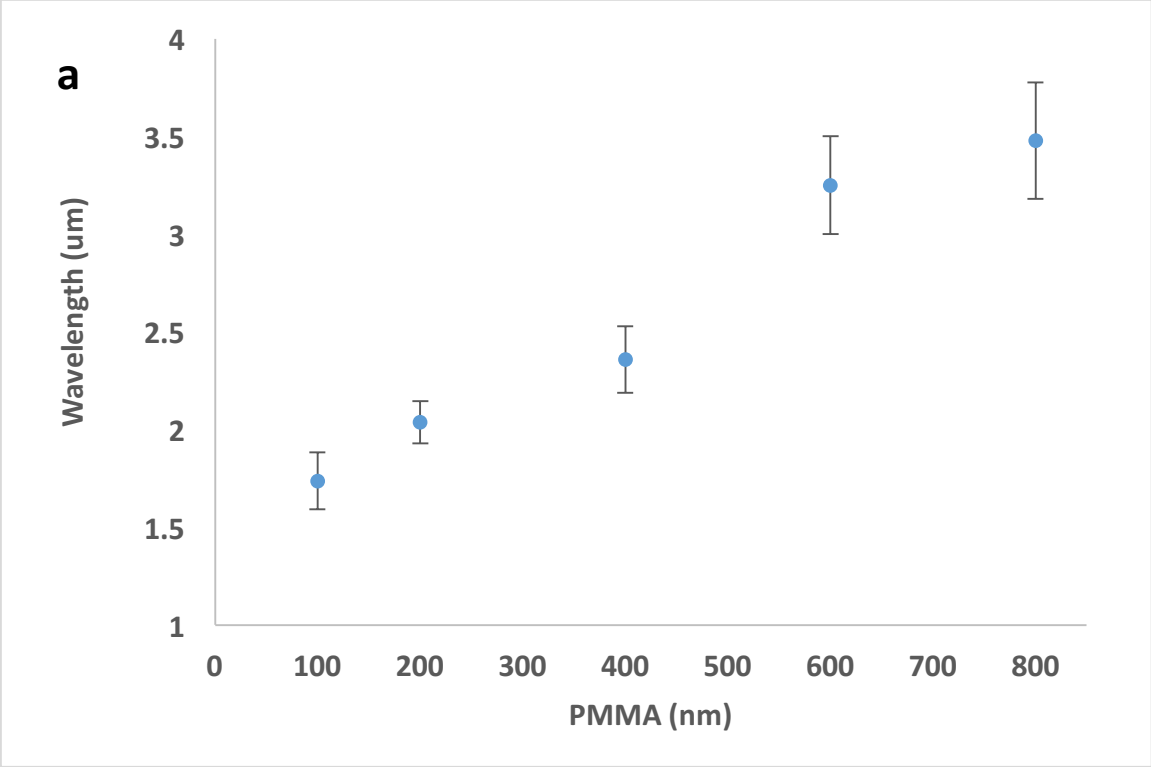

***Figure 18*. Measurement of Si Wrinkles. (a) Wavelength of the Si wrinkles.**

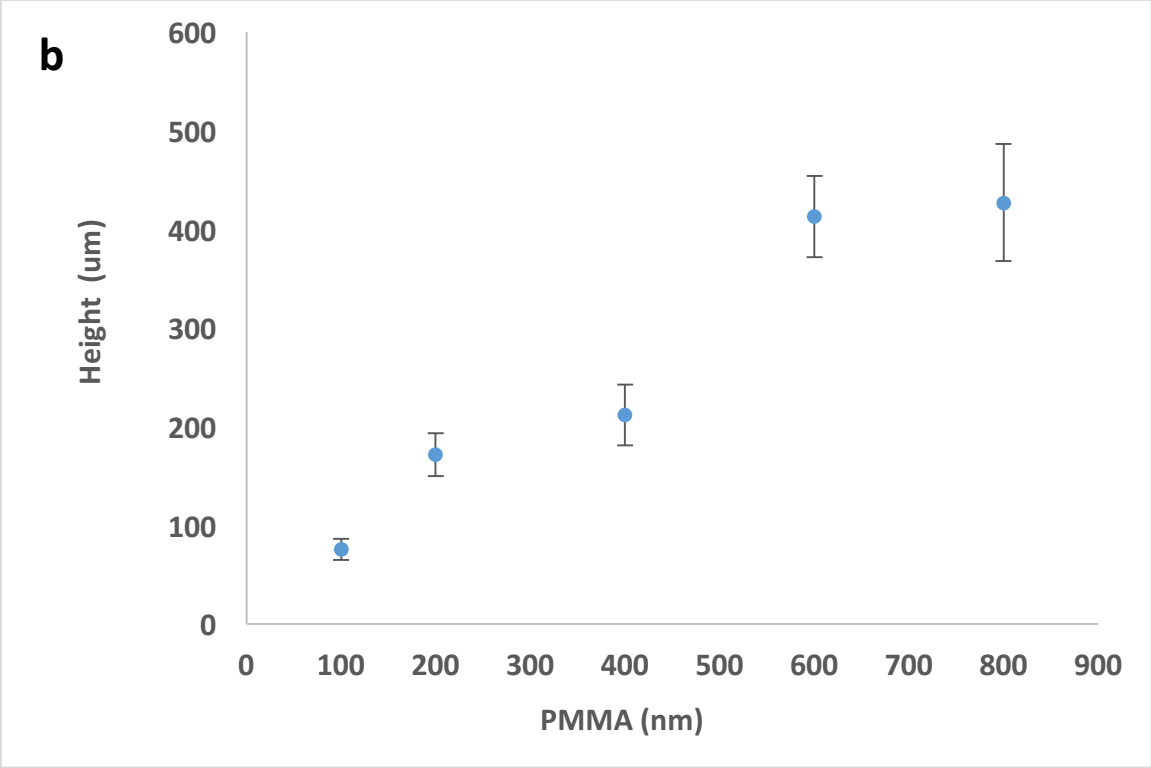

***Figure 18*. Measurement of Si Wrinkles. (b) Height of the Si wrinkles.**

Formation of Si wrinkles had a similar trend as the Al wrinkles. Discontinuous Si wrinkles and dots were observed with 100 nm of PMMA (Figure 17. a), and continuous Si wrinkles were found in 200 – 800 nm of PMMA (Figure 17. b – d). In contrast to Al wrinkles, Si wrinkles were easily formed with thin PMMA layers. Moreover, the wavelengths and heights of Si wrinkles were greater than the Al wrinkles (Figure 18) The Young's modulus of Si is greater that the Al, therefore deformation of Si is more favorable than Al.

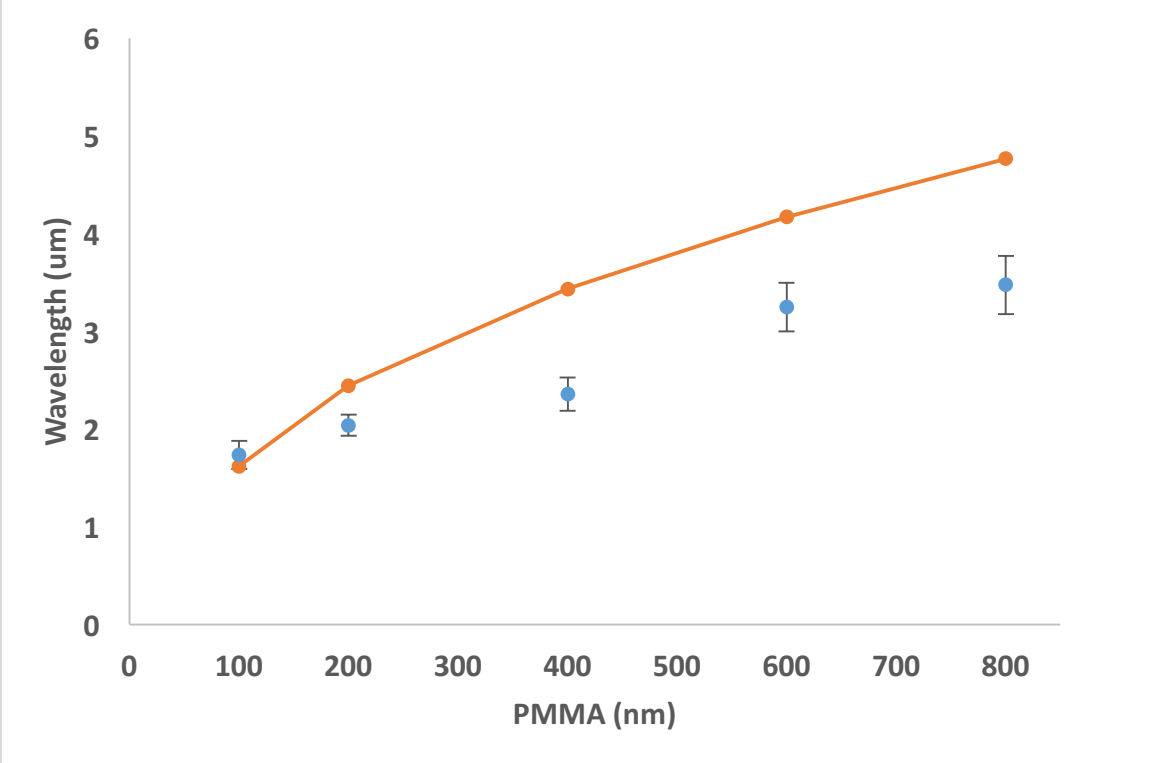

***Figure 19*. Comparison of Predicted and Measured Si Wrinkles. Predicted Si Wrinkles (Orange) and Measured Si Wrinkles (Blue dots).**

The wavelengths of Si wrinkles were simulated with the mathematic model to evaluate the Al wrinkles (Figure 14). The overall results were similar to predicting the wavelengths and heights of the Al wrinkles. Again, the model could be improved by obtaining the correct Young's modulus of PMMA and Si.

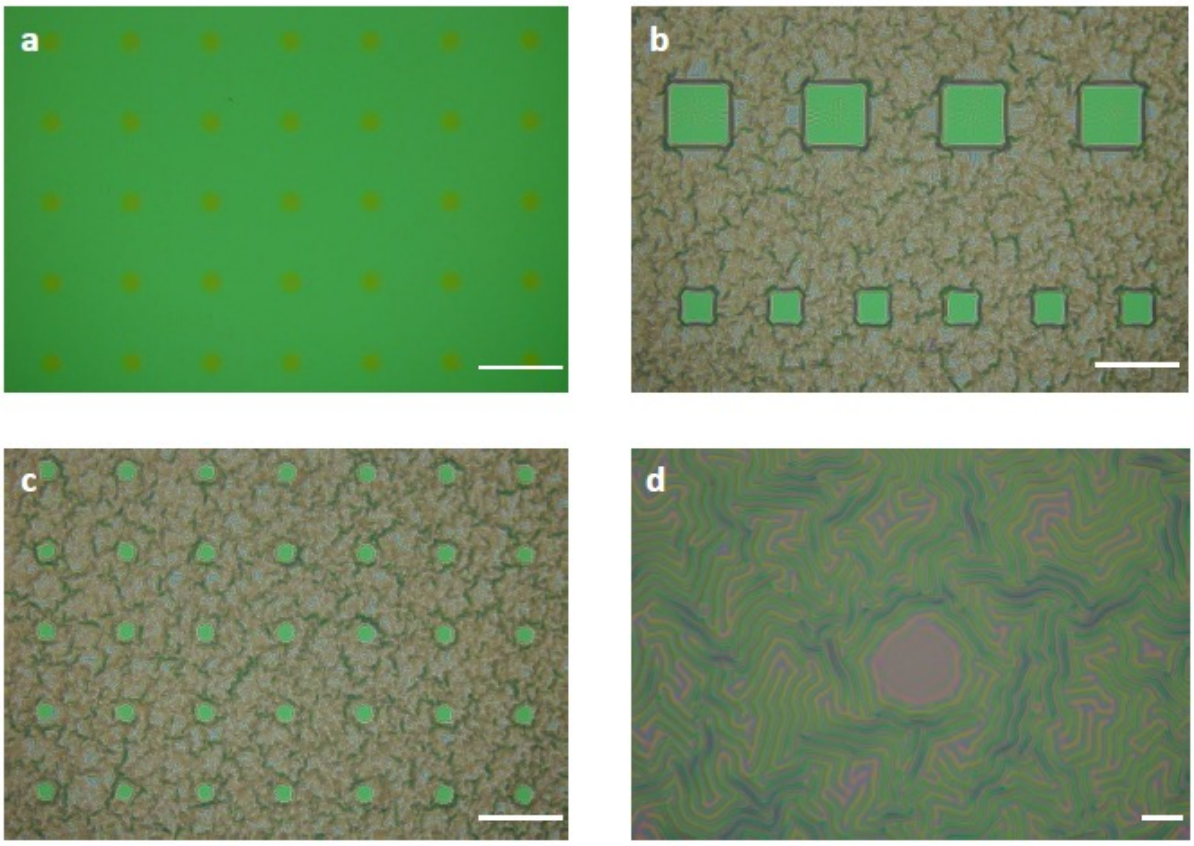

Figure 20. **Plasma Assisted Wrinkles (Type 1). The features were protected. Scale bars for a – c is 100 um, and scale bar for d is 10 um.**

A new technique inspired by Guo et al. was explored to control Si wrinkles [18]. The mechanism of creating the wrinkles is similar to bending. As the folding a single sheet of paper proves to be easier than a stack, and the folding of a tiny object more difficult than a large one, the same concept

was applied to the creation of Si wrinkles. The thickness of Si was controlled selectively by plasma etching and photolithography.

Type 1 Si wrinkles were created by depositing small features of photoresist (e.g. squares and circles) during dry etching. Si wrinkles were only found in the areas that were not protected by the photoresist. In the protected areas, the areas were smaller and thicker than the unprotected areas. Therefore, deformation of Si was not favorable in the protected areas.

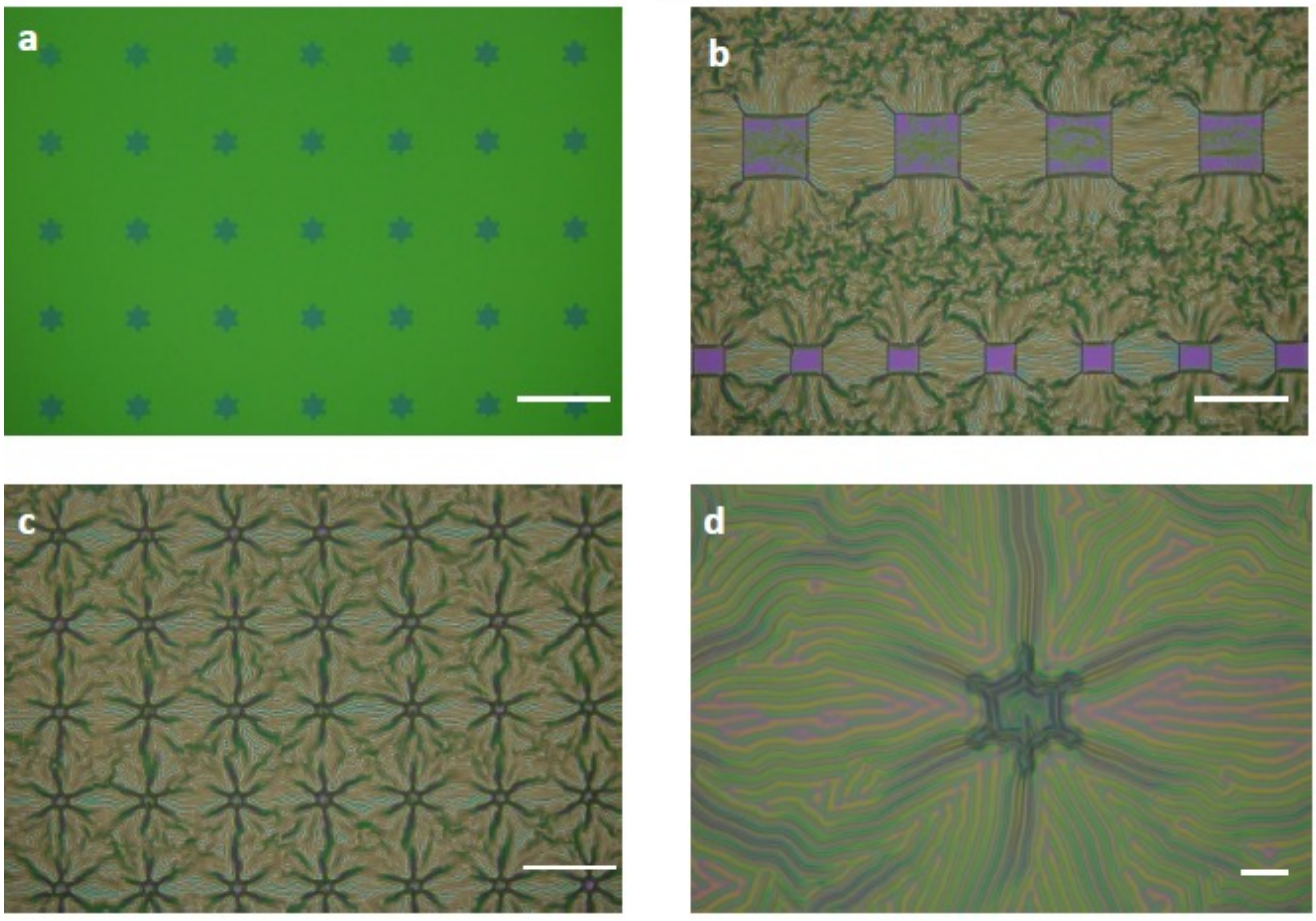

Figure 21. **Plasma Assisted Wrinkles (Type 2). The features were etched. Scale bars for a – c is 100 um, and scale bar for d is 10 um.**

Type 2 Si wrinkles were prepared by covering the majority area of photoresist with small openings (e.g. square and circles), and the Si was etched through the openings. Patterns of Si wrinkles were discovered, and the directions of the wrinkles can be controlled. Directional wrinkles in the protected area tended to develop at the sharp edges of the small features.

In contrast to type 1 wrinkles (Figure 20. b), type 2 wrinkles were found in the areas of the features (Figure 21. b). In the areas of the features, the thickness of the type 2 was thinner than the type 1, and only small amount of Si was etched in the type 2. Therefore, formation of type 2 wrinkles was favorable in the protected and unprotected areas.

2.4. Conclusion

In summary, random and aligned Al wrinkles demonstrated by Yoo et al can be reproduced by using PMMA rather than PS as the polymer layer. Also, the mathematics model that established by Yoo et al predicted the trend of the wavelengths of the Al wrinkles. The model contained an error percentage of 25%, accuracy could be improved should the Young's modulus of PMMA be measured. Also, experiments were conducted to investigate Si as the top layer. Si wrinkles can be generated using PMMA as the polymer layer, and patterned Si wrinkles were created by photolithography and plasma etching.

In the next chapter, coupling graphene and Si wrinkles were explored. An innovative method to transfer graphene on top of the Si/PMMA is discussed, and strain in graphene wrinkles analyzed by the Raman spectra.

Chapter 3. Nanoscale Graphene Wrinkles on Silicon

3.1. Introduction

Si wrinkles in chapter 2 was an ideal platform to study strain in graphene. In order to measure significant strain in graphene, nanoscale Si wrinkles must be generated. In previous studies, nanoscale Au wrinkles were produced by reducing the thickness of the top and polymer layers. The results agreed with the theoretical predictions. In this chapter, fabricating nanoscale Si wrinkles was explored, and strain in graphene on nanoscale Si wrinkles was characterized by Raman spectroscopy.

3.2. Experimental Section

Fabrication of Semiconductor and Polymer Bilayer

The bilayer was prepared by replicating the method discussed on chapter 2. Initially, 50 nm of PMMA, (950K A Resist) spun on top of a silicon wafer. The wafer was then baked at 125 ℃ for 1 minute.

Si with a thickness of 5 nm was deposited on top of the PMMA by thermal evaporation. Silicon wafers were used as the silicon source. Briefly, materials were deposited when the vacuum chamber reached 1×10^{-5} psi, and the deposition rate was maintained at 0.5 Å per second.

The bilayer was heated on top of a hot plate in an ambient environment for 24 hours, with the annealing temperature set to 120℃ (Figure. 9). The wrinkles were examined by optical microscopy and atomic force microscopy (AFM).

Wax Transfer Graphene

Paraffin wax was used as a carry layer instead of the conventional PMMA method. Wax solution (5%) was prepared by mixing hexane and paraffin wax. The wax was coated on top of the graphene/ copper foil by drop casting, and the foil was heated at 60 ℃ for 30 minutes. Since graphene was grown on both sides of the copper foil, the uncoated graphene was etched away by oxygen plasma at 60 watts for three minutes. To remove the copper, the foil was left on top of the $FeCl_3$ (1 M) solution for 60 minutes. A clean glass slide was used to transfer from the $FeCl_3$ to DI water. The wax and graphene layers were retrieved by inserting the bilayers substrate in the DI water. After the substrate was completely dry, the wax can be removed by hexane for overnight.

3.3. Results and Discussion

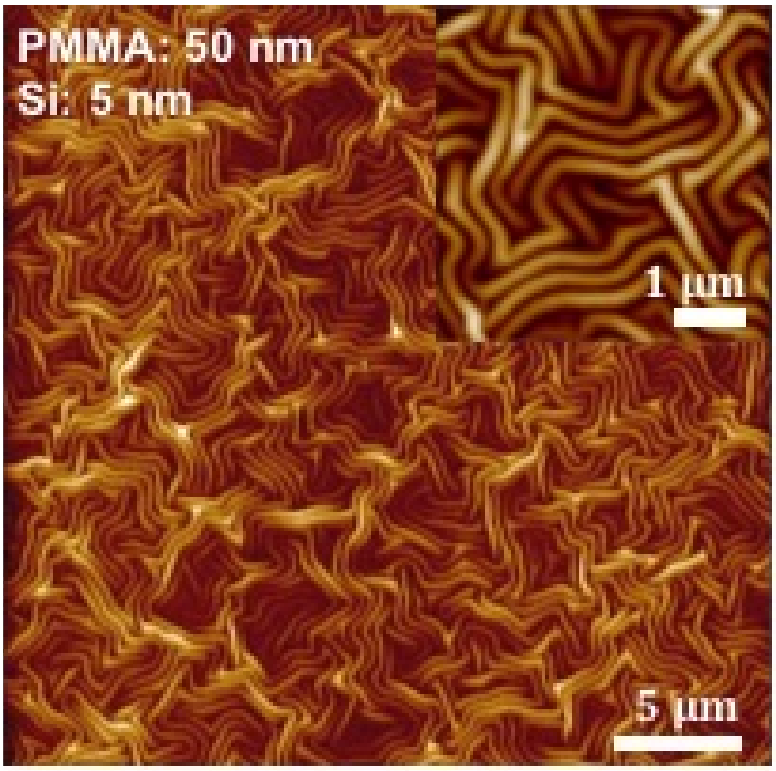

Figure 22 **AFM images of Si Nanowrinkles (5nm Si and 50 nm PMMA).**

Nanoscale Si wrinkles were produced by reducing the thickness of Si and PMMA (Figure 22), which agreed with the observations presented in Chapter 2. The wavelengths of the wrinkles were directly proportional to the thickness of PMMA. The theoretical and measured wavelength of the wrinkles are listed in Table 3. The theoretical wavelength was computed using the equation that was derived by Yoo et al, and the estimate contained about 16% error. The error percentage is to be expected when considering a rough estimation of the Young's modulus of PMMA.

Table 3. **Theoretical and Measured Wavelengths of Si Wrinkles (5nm Si/ 50 nm PMMA).**

	Wavelength (nm)
Theoretical [15]	346
Measured	291 ± 30

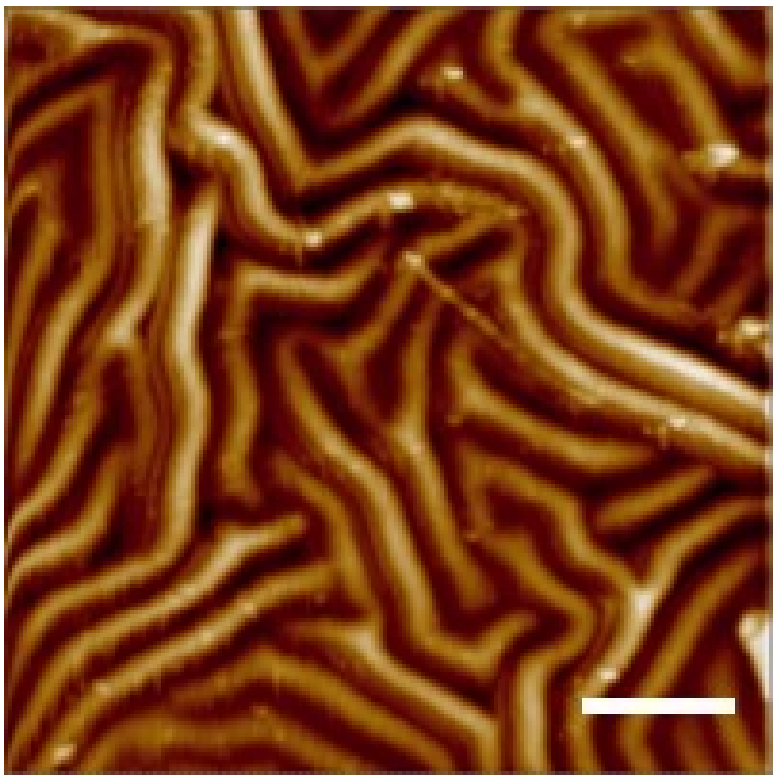

Figure 23. **Graphene on Si Nanowrinkles (5nm Si and 50 nm PMMA). The scale bar is 1 um.**

In contrast to the conventional method for transferring graphene which utilizes PMMA, graphene was instead transferred onto the bilayer with paraffin wax as a carrying film, eliminating the risk of damage to the bilayer posed by the use of acetone. Paraffin wax is soluble in hexane, and as hexane was compatible with the bilayer the quality of the Si wrinkles was not affected.

Graphene wrinkles were created by annealing the bilayer above the glass transition temperature of PMMA (Figure 23), and the AFM image suggesting that graphene adapted to the shape of the Si

wrinkles. To identify the strain in graphene, Raman spectra of flat and wrinkled graphene were measured.

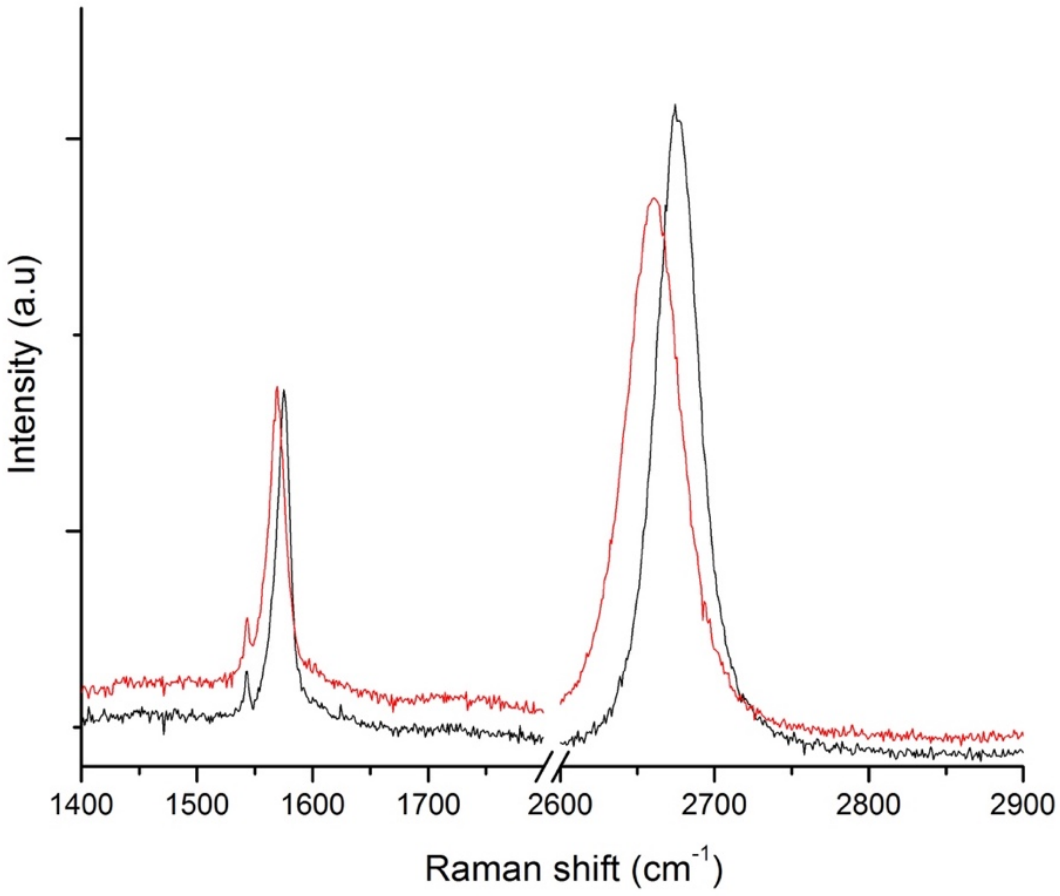

***Figure 24*. Raman Spectra of Nanoscale Si Wrinkles with Graphene. (Red-Wrinkles, Black-Flat)**

The Raman spectra of graphene wrinkles were red shifted, indicating that graphene was under tensile strain. The result confirmed our hypothesis that tensile strain in graphene can be created if the surface area of the substrate increased without shrinking the volume of the substrate. The tensile strain in graphene was quantified by OriginLab (Table 4).

Table 4. **Peak Positions of Flat and Wrinkled Graphene.**

	G band (cm^{-1})	2D band (cm^{-1})
Flat Graphene	1569.6409	2660.5562
Wrinkled Graphene	1574.0231	2676.4722

The positions of the G and 2D bands in Figure 24 were identified by OriginLab, and the tensile strain in graphene was estimated based on the shift of the 2D band. Ni et al found that graphene shifted about -27.1 cm^{-1} for every 1% of tensile strain [5], and the Si wrinkles created 0.6% of tensile strain in graphene.

3.4. Conclusion and Future Work

The creation of tensile strain in graphene was successfully demonstrated by adapting the shape of the Si nanowrinkles. Similar results were observed by Florio et al [12], and 0.45 % of tensile strain in graphene was measured. More tensile strain in graphene can be achieved by the Si nanowrinkles, and tensile strain in graphene was 0.6%.

For future work, systematic experiments will be required. Correlating the sizes of the Si wrinkles and the strain in graphene would yield information beneficial for the building of graphene devices, as band gaps and chemical reactivity of graphene can be modified by strains. Also, a better understanding of method in controlling anisotropic graphene wrinkles would be important for fabricating graphene devices. Non-invasive techniques such as plasma assisted wrinkles will be needed, especially in preventing damage to grapheme during the annealing process.

References

[1] Xia, F., Wang, H., Xiao, D., Dubey, M., & Ramasubramaniam, A. (2014). Two-dimensional material nanophotonics. *Nature Photonics,8*(12), 899-907. doi:10.1038/nphoton.2014.271

[2] Lee, S. K., Kim, H., & Shim, B. S. (2013). Graphene: an emerging material for biological tissue engineering. *Carbon letters,14*(2), 63-75. doi:10.5714/cl.2013.14.2.063

[3] Zang, J., Ryu, S., Pugno, N., Wang, Q., Tu, Q., Buehler, M. J., & Zhao, X. (2013). Multifunctionality and control of the crumpling and unfolding of large-area graphene. *Nature Materials,12*(4), 321-325. doi:10.1038/nmat3542

[4] Zhang, L., Yu, J., Yang, M., Xie, Q., Peng, H., & Liu, Z. (2013). Janus graphene from asymmetric two-dimensional chemistry. *Nature Communications, 4*, 1443. doi:10.1038/ncomms2464

[5] Ni, Z. H., Yu, T., Lu, Y. H., Wang, Y. Y., Feng, Y. P., & Shen, Z. X. (2008). Uniaxial Strain on Graphene: Raman Spectroscopy Study and Band-Gap Opening. *ACS Nano,2*(11), 2301-2305. doi:10.1021/nn800459e

[6] Bissett, M. A., Izumida, W., Saito, R., & Ago, H. (2012). Effect of Domain Boundaries on the Raman Spectra of Mechanically Strained Graphene. *ACS Nano,6*(11), 10229-10238. doi:10.1021/nn304032f

[7] Bissett, M. A., Konabe, S., Okada, S., Tsuji, M., & Ago, H. (2013). Enhanced Chemical Reactivity of Graphene Induced by Mechanical Strain. *ACS Nano,7*(11), 10335-10343. doi:10.1021/nn404746h

[8] Smith, A. D., Niklaus, F., Paussa, A., Schröder, S., Fischer, A. C., Sterner, M., . . . Lemme, M. C. (2016). Piezoresistive Properties of Suspended Graphene Membranes under Uniaxial and Biaxial Strain in Nanoelectromechanical Pressure Sensors. *ACS Nano,10*(11), 9879-9886. doi:10.1021/acsnano.6b02533

[9] Kumar, S., Kaushik, S., Pratap, R., & Raghavan, S. (2015). Graphene on Paper: A Simple, Low-Cost Chemical Sensing Platform. *ACS Applied Materials & Interfaces,7*(4), 2189-2194. doi:10.1021/am5084122

[10] Bao, W., Miao, F., Chen, Z., Zhang, H., Jang, W., Dames, C., & Lau, C. N. (2009). Controlled ripple texturing of suspended graphene and ultrathin graphite membranes. *Nature Nanotechnology,4*(9), 562-566. doi:10.1038/nnano.2009.191

[11] Hallam, T., Cole, M. T., Milne, W. I., & Duesberg, G. S. (2013). Field Emission Characteristics of Contact Printed Graphene Fins. *Small,10*(1), 95-99. doi:10.1002/smll.201300552

[12] Florio, G. D., Bründermann, E., Yadavalli, N. S., Santer, S., & Havenith, M. (2014). Graphene Multilayer as Nanosized Optical Strain Gauge for Polymer Surface Relief Gratings. *Nano Letters,14*(10), 5754-5760. doi:10.1021/nl502631s

[13] Lee, W., Kang, J., Chen, K., Engel, C. J., Jung, W., Rhee, D., . . . Odom, T. W. (2016). Multiscale, Hierarchical Patterning of Graphene by Conformal Wrinkling. *Nano Letters,16*(11), 7121-7127. doi: 10.1021/acs.nanolett.6b03415

[14] Okayasu, T., Zhang, H., Bucknall, D. G., & Briggs, G. A. (2004). Spontaneous Formation of Ordered Lateral Patterns in Polymer Thin-Film Structures. *Advanced Functional Materials,14*(11), 1081-1088. doi:10.1002/adfm.200305014

[15] Yoo, P.J., Suh, K.Y., Park, S.Y. and Lee, H.H. (2002), Physical Self-Assembly of Microstructures by Anisotropic Buckling. Adv. Mater., 14: 1383–1387. doi:10.1002/1521-4095(20021002)14:19<1383::AID-ADMA1383>3.0.CO;2-D

[16] Whitesides, G. M., Bowden, N., Brittain, S., Evans, A. G., & Hutchinson, J. W. (1998). *Nature,393*(6681), 146-149. doi:10.1038/30193

[17] Zhang, Z., Guo, C., Cao, S., Bai, L., Xie, Y., & Liu, Q. (2009). Ordered Metal Film Pattern with Submicron Period. *Japanese Journal of Applied Physics,48*(9), 090208. doi:10.1143/jjap.48.090208

[18] Guo, C. F., Nayyar, V., Zhang, Z., Chen, Y., Miao, J., Huang, R., & Liu, Q. (2012). Path-Guided Wrinkling of Nanoscale Metal Films. *Advanced Materials,24*(22), 3010-3014. doi:10.1002/adma.201200540

[19] Novoselov, K. S. (2004). Electric Field Effect in Atomically Thin Carbon Films. *Science,306*(5696), 666-669. doi:10.1126/science.1102896

[20] Takamura, M., Hibino, H., & Yamamoto, H. (2016). Applying strain into graphene by SU-8 resist shrinkage. *Journal of Physics D: Applied Physics,49*(28), 285303. doi:10.1088/0022-3727/49/28/285303

[21] Wang, Q., Hong, W., & Dong, L. (2016). Graphene "microdrums" on a freestanding perforated thin membrane for high sensitivity MEMS pressure sensors. *Nanoscale,8*(14), 7663-7671. doi:10.1039/c5nr09274d

[22] Jiang, T., Huang, R., & Zhu, Y. (2013). Interfacial Sliding and Buckling of Monolayer Graphene on a Stretchable Substrate. *Advanced Functional Materials,24*(3), 396-402. doi:10.1002/adfm.201301999

[23] Novoselov, K. S. (2004). Electric Field Effect in Atomically Thin Carbon Films. *Science,306*(5696), 666-669. doi:10.1126/science.1102896

[24] Gong, L., Kinloch, I. A., Young, R. J., Riaz, I., Jalil, R., & Novoselov, K. S. (2010). Interfacial Stress Transfer in a Graphene Monolayer Nanocomposite. *Advanced Materials,22*(24), 2694-2697. doi:10.1002/adma.200904264

[25] Haniff, M. A., Hafiz, S. M., Huang, N. M., Rahman, S. A., Wahid, K. A., Syono, M. I., & Azid, I. A. (2017). Piezoresistive Effect in Plasma-Doping of Graphene Sheet for High-Performance Flexible Pressure Sensing Application. *ACS Applied Materials & Interfaces,9*(17), 15192-15201. doi:10.1021/acsami.7b02833

[26] Tang, B., Guoxin, H., & Gao, H. (2010). Raman Spectroscopic Characterization of Graphene. *Applied Spectroscopy Reviews,45*(5), 369-407. doi:10.1080/05704928.2010.483886

[27] Shin, Y., Lozada-Hidalgo, M., Sambricio, J. L., Grigorieva, I. V., Geim, A. K., & Casiraghi, C. (2016). Raman spectroscopy of highly pressurized graphene membranes. *Applied Physics Letters,108*(22), 221907. doi:10.1063/1.4952972

[28] Wang, Q. H., Jin, Z., Kim, K. K., Hilmer, A. J., Paulus, G. L., Shih, C., . . . Strano, M. S. (2012). Understanding and controlling the substrate effect on graphene electron-transfer chemistry via reactivity imprint lithography. *Nature Chemistry,4*(9), 724-732. doi:10.1038/nchem.1421

[29] Frank, O., Tsoukleri, G., Parthenios, J., Papagelis, K., Riaz, I., Jalil, R., . . . Galiotis, C. (2010). Compression Behavior of Single-Layer Graphenes. *ACS Nano,4*(6), 3131-3138. doi:10.1021/nn100454w

[30] Deng, S., Gao, E., Wang, Y., Sen, S., Sreenivasan, S. T., Behura, S., . . . Berry, V. (2016). Confined, Oriented, and Electrically Anisotropic Graphene Wrinkles on Bacteria. *ACS Nano,10*(9), 8403-8412. doi:10.1021/acsnano.6b03214

[31] Ramasse, Q. M., Zan, R., Bangert, U., Boukhvalov, D. W., Son, Y., & Novoselov, K. S. (2012). Direct Experimental Evidence of Metal-Mediated Etching of Suspended Graphene. *ACS Nano,6*(5), 4063-4071. doi:10.1021/nn300452y

[32] Allain, A., Han, Z., & Bouchiat, V. (2012). Electrical control of the superconducting-to-insulating transition in graphene–metal hybrids. *Nature Materials,11*(7), 590-594. doi:10.1038/nmat3335

[33] Wang, M. C., Chun, S., Han, R. S., Ashraf, A., Kang, P., & Nam, S. (2015). Heterogeneous, Three-Dimensional Texturing of Graphene. *Nano Letters,15*(3), 1829-1835. doi:10.1021/nl504612y

Curriculum Vitae

Kam Sang (Mark) Kwok

Address: 3501 St Paul St, Baltimore, Maryland. **Tel**: 908-448-7254 **Email:** kkwok6@jhu.edu

EDUCATION

Johns Hopkins University — Baltimore, MD
Master of Science in Chemical & Biomolecular Engineering (GPA: 3.66/4.0) — Aug 2017
ChemBE Master's Essay Scholarship (Fall 2016, Spring 2017)
Advisor: Prof. Gracias, David

University of Illinois at Urbana- Champaign — Urbana- Champaign, IL
Bachelor of Science in Chemical & Biomolecular Engineering — Aug 2013
Advisor: Prof. Yang, Hong

PROFESSIONAL EXPERIENCE

Gracias Laboratory, Johns Hopkins University — Baltimore, MD
Research Assistant — July 2015 - Present
Master Thesis: Anisotropic Wrinkles of Graphene on Metal and Semiconductor Surfaces

- Introduced tensile strain in graphene by creating wrinkles of the silicon substrate
- Directed wrinkles of silicon by plasma etching and photolithography

Sigma-Aldrich, a part of MilliporeSigma, a business of Merck KGaA — St. Louis, MO
Biotech Production Intern — May 2016 – Aug 2016
Project Name: Development of Standardized Work Practices

- Recommended solutions to improve the cell media filling process to save $120k annually
- Proposed a new layout of the factory to reduce waste of motion
- Created statistical models to evaluate the performance of operators
- Collaborated with manufacturing manager, 4 supervisors and 20 operators to identify least efficient processes
- Conducted meetings with the operation and manufacturing managers to present the analysis of the facility
- Presented the significance of my study to the company at the intern poster session

Hong Yang Research Group, University of Illinois at Urbana- Champaign — Urbana- Champaign, IL
Research Assistant — May 2012 – May 2015

- Formulated crumpled and flat palladium nanosheets via "bottom- up" to compare their hydrogen sensing performance
- Developed a process to wrap HepG2 cells with different functionalized palladium nanosheets to study the cytotoxicity of the nanosheets
- Examined fuel cell activity of the crumpled and flat palladium nanosheets through cyclic voltammetry

PUBLICATIONS AND PATENTS

1. Y.-T. Pan‡, C. Smith‡, K. S. Kwok‡, J. R. Chen, H. J. Kong, H. Yang, "Functionalized ultrathin palladium nanosheets as patches for HepG2 cancer cells, ChemComm, **2015**, 51, 14171-14174. (‡: equal contribution)
2. Y. -T. Pan, X. Yin, K. S. Kwok, H. Yang, Higher-Order Nanostructures of Two-Dimensional Palladium Nanosheets for Fast Hydrogen Sensing, *Nano Lett*., **2014**, 14, 5953-5959.
3. H. Yang, K.S Kwok, Two- Dimensional Palladium Nanosheets for Fast Hydrogen Sensing, US Patent (Submitted)

SKILLS

Materials Synthesis and Characterization: Scanning Electron Microscope, Energy- Dispersive X-ray Spectroscopy, Langmuir- Blodgett Trough, UV-Vis, Cyclic Voltammetry, Mask Aligner, Physical Vapor Deposition, Spin Coater, Photolithography, Soft lithography, Plasma etcher
Cell Culture: Mammalian Cell Culture, 2D and 3D Cell Cultures, Gel Electrophoresis
Computer: MATLAB, COMSOL, CHEMCAD, MS Excel, Adobe Photoshop, AutoCAD
Language: Cantonese (native language), English (fluent), Mandarin (fluent)